



# Analysis of the Role of N-Linked Glycosylation in Cell Surface Expression, Function, and Binding Properties of SARS-CoV-2 Receptor ACE2

Raymond Rowland,<sup>a</sup>  Alberto Brandariz-Nuñez<sup>a</sup>

<sup>a</sup>Department of Pathobiology, College of Veterinary Medicine, University of Illinois at Urbana-Champaign, Urbana, Illinois, USA

**ABSTRACT** Human angiotensin I-converting enzyme 2 (hACE2) is a type I transmembrane glycoprotein that serves as the major cell entry receptor for SARS-CoV and SARS-CoV-2. The viral spike (S) protein is required for the attachment to ACE2 and subsequent virus-host cell membrane fusion. Previous work has demonstrated the presence of N-linked glycans in ACE2. N-glycosylation is implicated in many biological activities, including protein folding, protein activity, and cell surface expression of biomolecules. However, the contribution of N-glycosylation to ACE2 function is poorly understood. Here, we examined the role of N-glycosylation in the activity and localization of two species with different susceptibility to SARS-CoV-2 infection, porcine ACE2 (pACE2) and hACE2. The elimination of N-glycosylation by tunicamycin (TM) treatment, or mutagenesis, showed that N-glycosylation is critical for the proper cell surface expression of ACE2 but not for its carboxypeptidase activity. Furthermore, nonglycosylable ACE2 was localized predominantly in the endoplasmic reticulum (ER) and not at the cell surface. Our data also revealed that binding of SARS-CoV or SARS-CoV-2 S protein to porcine or human ACE2 was not affected by deglycosylation of ACE2 or S proteins, suggesting that N-glycosylation does not play a role in the interaction between SARS coronaviruses and the ACE2 receptor. Impairment of hACE2 N-glycosylation decreased cell-to-cell fusion mediated by SARS-CoV S protein but not that mediated by SARS-CoV-2 S protein. Finally, we found that hACE2 N-glycosylation is required for an efficient viral entry of SARS-CoV/SARS-CoV-2 S pseudotyped viruses, which may be the result of low cell surface expression of the deglycosylated ACE2 receptor.

**IMPORTANCE** Understanding the role of glycosylation in the virus-receptor interaction is important for developing approaches that disrupt infection. In this study, we showed that deglycosylation of both ACE2 and S had a minimal effect on the spike-ACE2 interaction. In addition, we found that the removal of N-glycans of ACE2 impaired its ability to support an efficient transduction of SARS-CoV and SARS-CoV-2 S pseudotyped viruses. Our data suggest that the role of deglycosylation of ACE2 on reducing infection is likely due to a reduced expression of the viral receptor on the cell surface. These findings offer insight into the glycan structure and function of ACE2 and potentially suggest that future antiviral therapies against coronaviruses and other coronavirus-related illnesses involving inhibition of ACE2 recruitment to the cell membrane could be developed.

**KEYWORDS** ACE2 glycoprotein, ACE2-spike binding, N-glycosylation, coronavirus, syncytium formation, virus entry

Responsible for the current pandemic (1–7), severe acute respiratory syndrome coronavirus-2 (SARS-CoV-2) is a highly transmissible betacoronavirus that emerged in 2019. Outcomes of human infection range from asymptomatic infection to severe clinical disease (8, 9). Infection is frequently associated with severe acute respiratory

**Citation** Rowland R, Brandariz-Nuñez A. 2021. Analysis of the role of N-linked glycosylation in cell surface expression, function, and binding properties of SARS-CoV-2 receptor ACE2. *Microbiol Spectr* 9:e01199-21. <https://doi.org/10.1128/Spectrum.01199-21>.

**Editor** Ujjwal Neogi, Karolinska Institutet

**Copyright** © 2021 Rowland and Brandariz-Nuñez. This is an open-access article distributed under the terms of the [Creative Commons Attribution 4.0 International license](https://creativecommons.org/licenses/by/4.0/).

Address correspondence to Alberto Brandariz-Nuñez, [Brandari@illinois.edu](mailto:Brandari@illinois.edu).

**Received** 6 August 2021

**Accepted** 13 August 2021

**Published** 8 September 2021

syndrome (SARS) but may also trigger other responses leading to multiorgan failure and death (5–7, 10–12). Several vaccines against SARS-CoV-2, approved for emergency use, are being administered to the global population. Currently, vaccines are highly effective and the most effective strategy for controlling this disease. Concerns about vaccine escape variants and the broad tropism of the virus require the continued pursuit of a broad range of antiviral strategies (13–15).

SARS-CoV-2 infection begins with the binding of the virus spike (S) protein to the cell surface receptor, angiotensin I-converting enzyme 2 (ACE2), which results in the fusion of the viral and cell membranes and viral entry (4, 16–19). Other cell surface molecules, such as heparin sulfate, may also contribute to the infection (20). ACE2 also serves as a receptor for SARS-CoV that was identified and isolated in 2002 (21). The S protein contains 22 N-glycosylation sites, which play important roles in immune evasion, protein conformation, and cell tropism (17–19, 22–24). One of the unique properties of the SARS-CoV-2 S protein is the presence of a furin-specific cleavage site located between the S1 and S2 subunits, which may assist in viral entry (25–27). In addition, other host enzymes, including TMPRSS2 (transmembrane protease, serine 2), might contribute to viral entry of the virus (16, 25–28).

Human ACE2 (hACE2) is a type I transmembrane glycoprotein that catalyzes the hydrolysis of angiotensin II (a vasoconstrictor peptide) into angiotensin (1–7, 29). hACE2 is composed of extracellular, transmembrane, and cytosolic domains (30, 31). The receptor contains 7 N-linked glycosylation sites, at amino acid residues 53, 90, 103, 322, 432, 546, and 690 (Fig. 1A) (30, 32–36). The sugar residues were confirmed by glycosidase treatment and glycomic and glycoproteomic analysis (32–36). The presence of an O-glycosylation site at T730 was also reported (34). One function that has been proposed for the N-linked glycans is a direct modulation of spike-hACE2 binding (34–36). In particular, the glycans of hACE2 at N90, N322, and N546 are all reported to interact with the SARS-CoV-2 S protein (35, 36). Recent studies evaluated the contribution of hACE2 N-glycosylation in the interaction with SARS-CoV-2 viral S protein (37, 38). The structures of the sugars on the hACE2 receptor were modified genetically or enzymatically, generating different hACE2 glycoforms (37, 38). They concluded that S binding with ACE2 is slightly influenced by the N-linked glycans present in the hACE2 receptor and that the hACE2 glycans play no role in viral entry (37, 38). However, the N-linked sugars present on the spike protein were critical for the virus to enter the host cells (38, 39).

ACE2 from different species possesses different glycosylation patterns (34), which may influence the tropism of the virus. For instance, the mouse ACE2 receptor, which is not susceptible to SARS-CoV-2 infection (4, 40), has only three N-glycosylation sites that share similarities with hACE2 (34). On the other hand, the porcine ACE2 (pACE2) receptor has eight potential N-glycosylation sites and shares four similar sites with hACE2 (Fig. 1A). *In vitro* studies found that the expression of pACE2 receptor on non-permissive cells to SARS-CoV-2 infection enables viral entry and infection (4, 40). In addition, there is growing evidence that pigs might be susceptible to SARS-CoV (41) or SARS-CoV-2 infection (42), although the results of these studies contradict previous reports that indicate that swine are not susceptible to SARS-CoV (43) or SARS-CoV-2 infections (44, 45). Based on these results, we compare the binding properties of hACE and pACE in response to deglycosylation.

It has been extensively proposed that N-glycosylation is involved in many important biological processes, including protein folding, enzymatic activity, trafficking, and cell surface expression of proteins (46, 47). However, the importance of N-glycosylation for ACE2 function has not been investigated previously. This work explores the role of N-glycosylation of both pACE2 and hACE2 receptors in the cell surface expression and activity and in regulating direct spike-ACE2 interactions. The results show that the total loss of glycans inhibits the proper cell surface expression of ACE2 but does not interfere with enzymatic activity. Additionally, the complete removal of glycans from both S and ACE2 proteins does not inhibit their binding. Interestingly, hACE2 N-glycosylation decreased cell-to-cell fusion

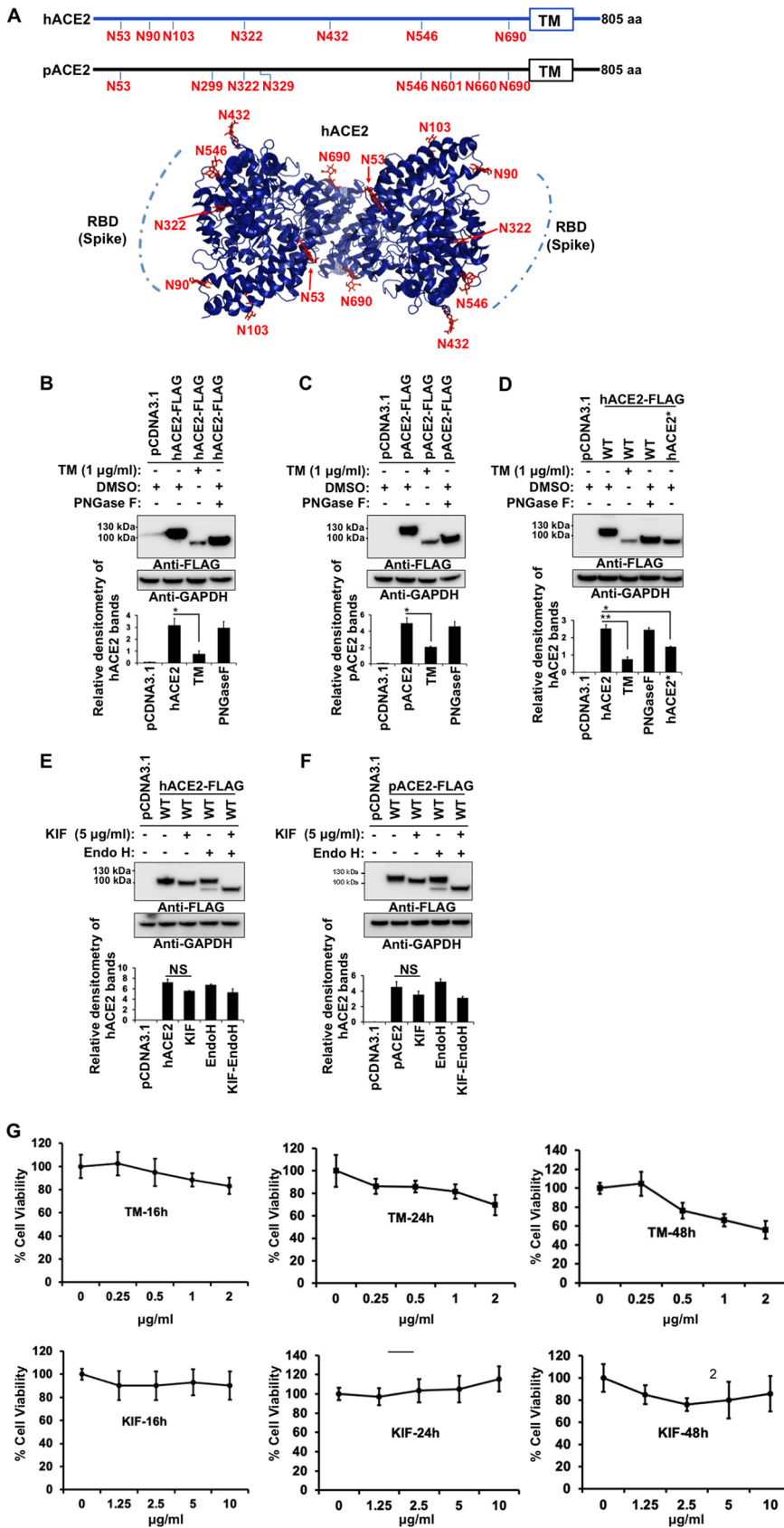


**FIG 1** Effect of N-glycosylation inhibition on expression and electrophoretic mobility of hACE2 and pACE2. (A) Schematic representations of the N-glycosylation sites of ACE2 receptors from human and (Continued on next page)

mediated by SARS-CoV S protein but not SARS-CoV-2 S protein-induced membrane fusion. Finally, we found that the presence of N-glycans in hACE2 is required for an efficient viral entry of SARS-CoV/SARS-CoV-2 S pseudotyped viruses, which can be attributed to the fact that deglycosylated ACE2 is less available in the cell surface.

## RESULTS

**N-glycosylation inhibition induces accumulation of ACE2 in the ER.** To understand the role of glycosylation in ACE2 function, we incorporated two N-glycosylation inhibitors: tunicamycin (TM) and kifunensine (KIF). TM inhibits the first step of N-glycan biosynthesis, which results in the complete absence of glycan residues (48), while KIF is an inhibitor of endoplasmic reticulum (ER)-located mannosidase I and complex N-glycosylation, which results in the production of glycoproteins lacking the characteristic terminal sugar found on mature N-glycans (48, 49). Immunoblot analysis of whole-cell lysates was performed following transfection of 293T cells with a hACE2-expressing plasmid and treatment with TM. Treatment of cells with TM resulted in a faster electrophoretic mobility shift for the hACE2 band, showing the loss of N-linked glycosylation (Fig. 1B, lane 3). Digestion of untreated cell lysates with peptide-N-glycosidase F (PNGase F), which cleaves all N-glycans, resulted in a hACE2 band similar in size to that of TM-treated cells. These results confirm the deglycosylation of hACE2 (Fig. 1B, lane 4). Similar results were obtained when we performed the same experiments with pACE2 (Fig. 1C). To further confirm that TM treatment and PNGase F digestion produced an N-glycosylation-deficient hACE2, we generated a hACE2 variant, in which all the N present in the consensus N-glycosylation sites were replaced by Q (for clarity, this new mutant is herein referred to as hACE2\*). As expected, expression of hACE2\* in 293T cells resulted in detection of a band with a molecular weight similar to that of TM-treated lysates or samples digested with PNGase F (Fig. 1D, lane 5). Interestingly, TM treatment showed reduced levels of ACE2 (Fig. 1B to D). The effect of TM was mimicked by hACE2\* construct, which lacked glycans. Together, these data suggest that core N-glycosylation is important for ACE2 biosynthesis. As a control, we used the MTS [3-(4,5-dimethylthiazol-2-yl)-5-(3-carboxymethoxyphenyl)-2-(4-sulfophenyl)-2H-tetrazolium] assay (50, 51) to show that the TM concentration utilized in our experiments, for an incubation time of 16 h, was not toxic to cells (cell viability of ~88%) (Fig. 1G).

KIF treatment of transfected cells did not have a significant impact on the electrophoretic mobility of either hACE2 or pACE2 and generated bands with a slightly shorter molecular weight (Fig. 1E and F, lane 3). However, the digestion of KIF-treated cell lysates with endo- $\beta$ -N-acetylglucosaminidase H (endo H), which cleaves only the

### FIG 1 Legend (Continued)

Fig. The hACE2 N-linked glycosylation sites, -Asn-Xaa-Ser/Thr-(Xaa $\neq$ P)-, are indicated in red. Eight potential N-glycosylation sites in the pACE2 are also indicated in red. The box is the transmembrane domain. A three-dimensional (3D) model showing the location of N-glycans on hACE2 dimer (PDB ID: 6M18) is shown. The potential binding location of SARS-CoV-2 receptor-binding domain (RBD) with hACE2 receptor is also shown. Recent molecular dynamics simulation studies using full glycan structures indicate that N-glycans at N90, N322, and N546 may be implicated in the interaction with coronavirus S protein RBD (35, 36). (B and C) HEK 293T cells were transfected with plasmids expressing either hACE2 (B) or pACE2 (C) and treated with TM for 16 h before harvesting or digested with PNGase F. ACE2 was detected with anti-FLAG antibody. (D) Western blotting of hACE2 and hACE2\* expression levels in transfected HEK 293T cells. Cells were treated with TM, and cell lysates were digested with PNGase F. (E and F) Western blots of hACE2 and pACE2 expression levels after KIF treatment for 16 h. Cell lysates were digested with endo H and immunoblotted with anti-FLAG antibody. In all experiments, GAPDH was used as a loading control. Densitometry of ACE2 bands shown in B through F are normalized to the loading control GAPDH. Fold changes are shown relative to empty vector (pCDNA3.1), and results are means  $\pm$  standard deviation (SD) values from three independent experiments (\*,  $P < 0.05$ ; \*\*,  $P < 0.005$ ; NS, not significant). hACE2\* refers to N-glycosylation sites removed by replacing Asn with Gln. (G) Cell viability was determined by measuring the reduction of the water-soluble tetrazolium dye MTS to water-soluble colored formazan product. We treated  $3 \times 10^4$  HEK 293T cells/well in a 96-well plate with the indicated concentrations of tunicamycin (TM) or kifunensine (KIF) for 16 h, 24 h, or 48 h at 37°C. After the incubation periods, 20  $\mu$ l MTS solution was added to each well for an additional 2 h at 37°C. The optical density was measured at 490 nm using a microplate reader. Results are means  $\pm$  SD values from three independent experiments. Mock-treated cells represent 100% viability.

high-mannose and hybrid branches of N-glycans, resulted in bands at a molecular weight lower than that of untreated controls (Fig. 1E and F, lane 5). Moreover, untreated cell lysates digested with endo H produced two different bands for both ACE2 proteins, one band with a molecular weight similar to that of the control and a faint band with the same size as that of the KIF-treated cells (Fig. 1E and F, lane 4). These last results confirmed a small presence of high-mannose/hybrid type glycans on both ACE2 receptors. Taken together, these results suggest that ACE2 contains complex-form and high-mannose N-linked structures, which are consistent with previous studies (32–35). As a control, we utilized the MTS assay test (50, 51) to show that the KIF concentration used in our experiments, for an incubation time of 16 h, was not toxic to cells (cell viability of ~93%) (Fig. 1G).

Since the blocking of N-glycosylation might cause the accumulation of unglycosylated proteins in the ER (46, 47), we tested the effect of N-glycosylation inhibition on the subcellular localization of ACE2. For this experiment, we studied the localization of ACE2 by immunofluorescence in the presence of TM or KIF. As shown in Fig. 2A, TM treatment induced colocalization of human and porcine ACE2 proteins with an ER marker, PDI (52, 53). In the absence of TM, the ACE2 proteins were localized mostly in the cell surface and showed no accumulation in the ER (Fig. 2A). Similarly, incubation of the cells with the mannosidase I inhibitor, KIF, had little or no effect on the cell surface localization of ACE2 (Fig. 2B). These observations indicate that the mannosidase I activity, which is required for processing newly formed high-mannose glycoproteins in the ER into mature glycoproteins containing highly hybrid complex-type glycans (46), is not necessary for the cell surface expression of ACE2. Quantification of the colocalization between the ACE2 proteins and the ER marker verified the accumulation of the ACE2 in the ER after TM treatment (Fig. 2C).

To further confirm that the N-glycosylation-deficient ACE2 proteins were arrested in the ER, we used a Golgi marker, golgin-97. As shown in Fig. 2D, TM treatment did not induce an overlap with the Golgi marker, confirming that the N-glycosylation-defective ACE2 proteins were trapped in the ER and unable to progress down the normal secretory pathway through the Golgi apparatus. Collectively, our data suggest that N-glycosylation is critical for cell surface expression of ACE2.

**N-glycosylation-deficient hACE2 variants accumulate in the ER.** Since TM is non-specific, affecting the glycosylation of all proteins, we repeated the same localization experiments by constructing ACE2 proteins lacking different glycosylation sites. Mutants were constructed by replacing N with a Q. Immunoblot analysis on whole-cell lysates was performed following transfection of 293T cells with the hACE2 mutant constructs. The highest-molecular-weight band was found in the wild-type protein. As the number of N-glycosylation sites decreased, the migration size was reduced (Fig. 3A). Next, we investigated the cellular distribution of the N-glycosylation-deficient mutants expressed in 293T cells by immunofluorescence. The results revealed that the triple and quadruple mutants were expressed mostly on the cell surface, similar to the wild-type hACE2 (Fig. 3B and C). Colocalization of the quadruple mutant and ER was also observed in some cells (Fig. 3B and C), whereas the other mutants, in which most or all of the N-glycosylation sites were removed, overlapped strongly with the ER (Fig. 3B and C). These results indicate that the N-glycosylation-deficient hACE2 variants failed to exit in the ER and, in turn, were not expressed at the cell surface. To further verify that N-glycosylation-defective ACE2 variants accumulated in the ER, we next tested whether these variants colocalized with the ER chaperone, calnexin (54). ACE2 nonglycosylated forms and calnexin colocalized (Fig. 3D), confirming that N-glycosylation-deficient ACE2 variants accumulated in the ER. Finally, to further corroborate that hACE2\* is retained in the ER, we analyzed its colocalization with golgin-97. As shown in Fig. 2D, hACE2\* did not overlap the Golgi marker, verifying that the N-glycosylation-deficient hACE2 variant was retained in the ER and unable to progress down the normal secretory pathway through the Golgi apparatus. Altogether, our results indicate that at least partial N-glycosylation is necessary for the proper cell surface expression of hACE2.

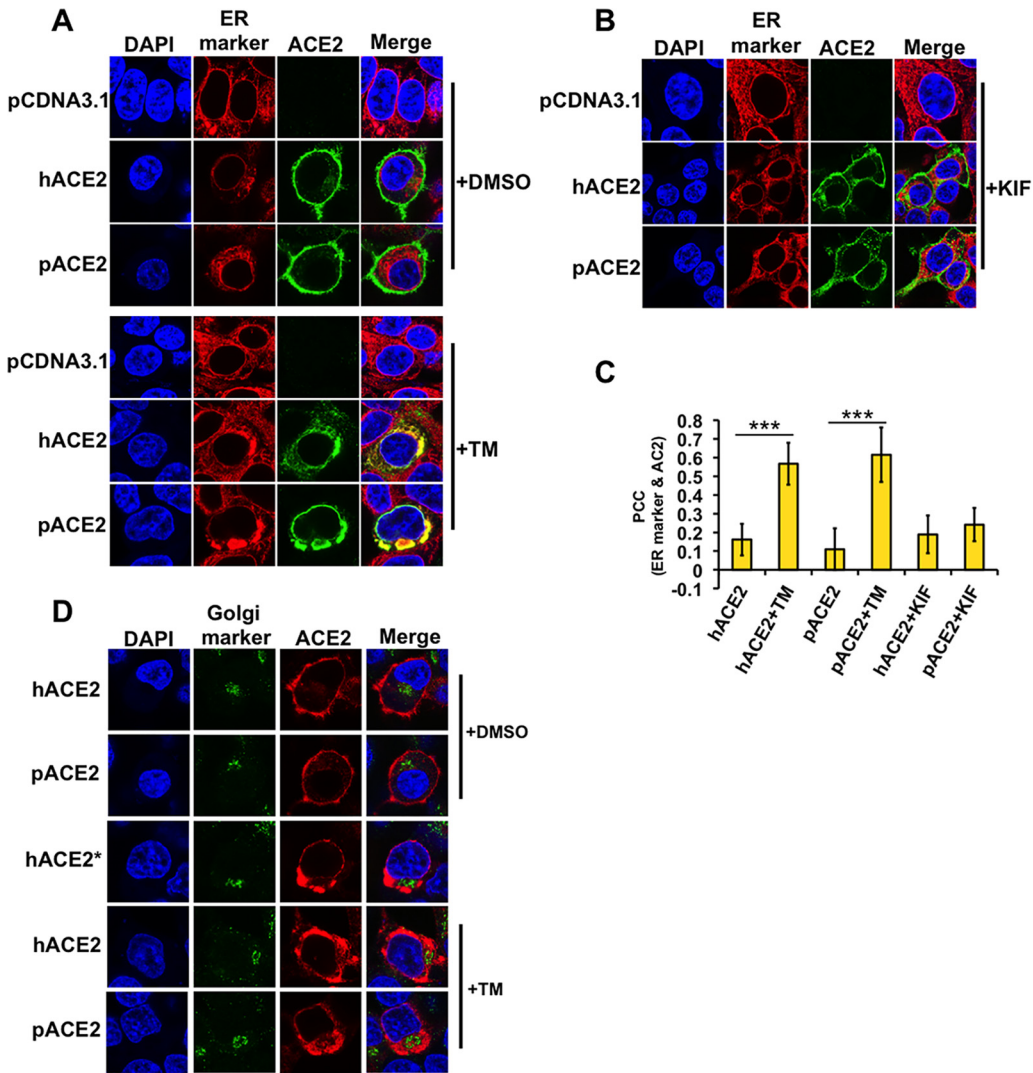


**FIG 2** Inhibition of cellular N-glycosylation induces colocalization of ACE2 with the ER. (A) Semiconfluent monolayers of HEK 293T cells grown on coverslips were transfected with either hACE2- or pACE2-expressing plasmids, and the cells were incubated with TM (1  $\mu$ g/ml) (+TM) dissolved in DMSO or DMSO only (+DMSO) for 16 h, fixed, and stained with anti-FLAG antibody and then with Alexa 488-goat anti-rabbit IgG (green). ER was visualized by staining cells with PDI monoclonal antibody, followed by Alexa 594-goat anti-mouse IgG (red). Nuclei were counterstained with DAPI (blue). (B) Same as panel A, except cells were treated with KIF (5  $\mu$ g/ml) (+KIF) for 16 h. (C) Quantification of colocalization of ACE2 proteins and ER. Five to six fields were randomly selected in each sample and 50 to 60 individual cells were analyzed. Pearson's correlation coefficient (PCC) values are means  $\pm$  SD from one representative experiment performed in triplicate. \*\*\*,  $P < 0.0005$  with respect to hACE2 and pACE2. Similar results were obtained in three separate experiments and representative data are shown. (D) HEK 293T cells were transfected with either hACE2- or hACE2\*-expressing plasmids, as well as pACE2-expressing vector. Transfected cells were either untreated (+DMSO) or incubated with TM (1  $\mu$ g/ml) dissolved in DMSO (+TM) for 16 h. All cells were fixed and immunostained using anti-M2 FLAG antibody and then with Alexa 594-conjugated goat anti-mouse IgG (red). Golgi apparatuses were visualized by immunostaining them with a golgin-97 antibody, followed by Alexa 488-conjugated goat anti-rabbit IgG (green). Nuclei were counterstained with DAPI (blue). Similar results were obtained in three separate experiments and representative data are shown.

**N-glycosylation is critical for the proper cell surface expression of ACE2.** The previous immunofluorescence experiments suggested that cell surface expression of the ACE2 nonglycosylated variants, generated either by TM treatment (Fig. 2) or by mutagenesis (Fig. 3), was reduced compared with that of wild-type ACE2. The abundance of nonglycosylated ACE2 or wild-type ACE2 on the cell surface was analyzed by cell surface biotinylation. As shown in Figure 4A and B, the surface density for both hACE2 and pACE2 proteins produced following TM treatment was significantly reduced compared with that of untreated cells. Similarly, the presence of the hACE2\*

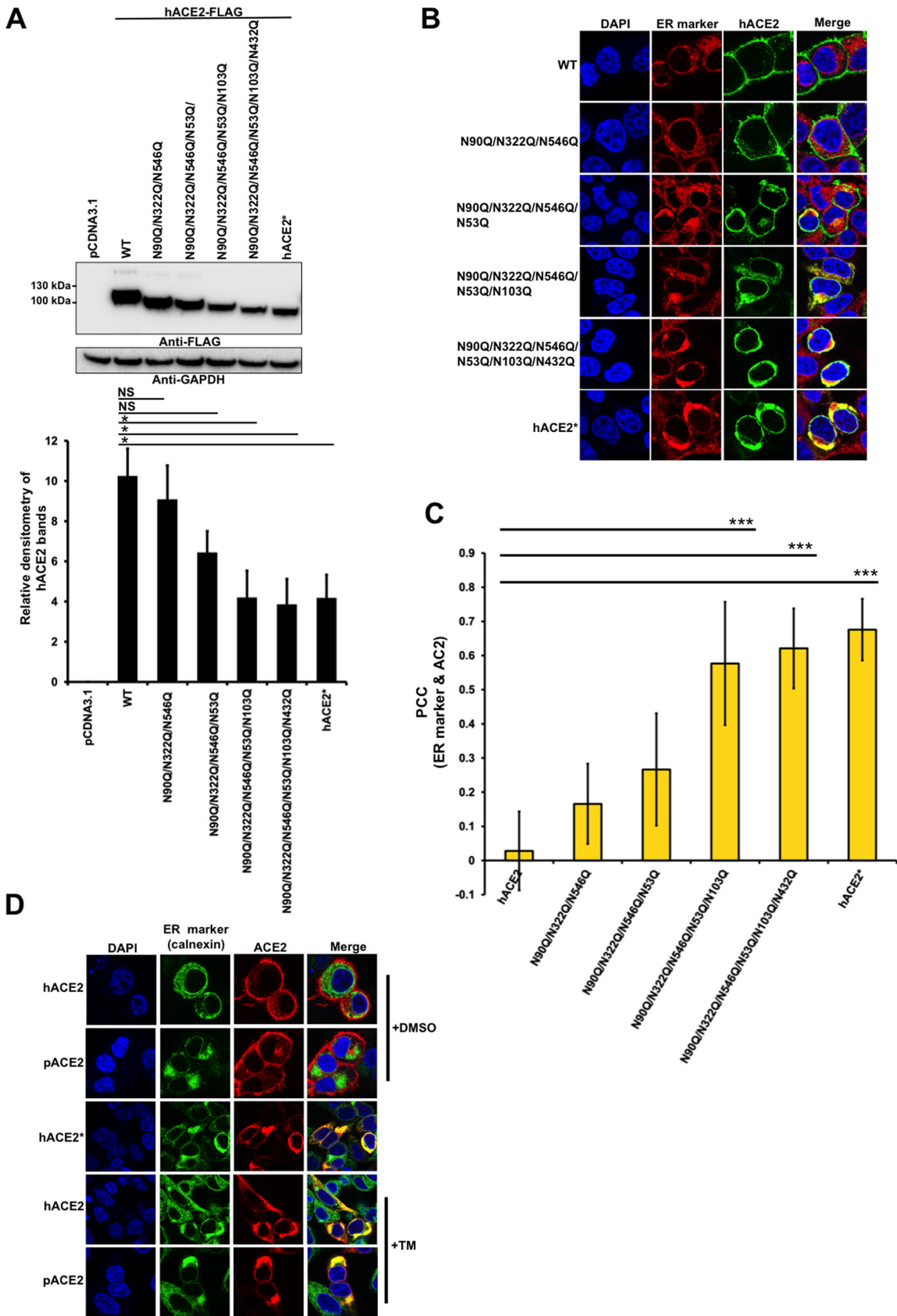


**FIG 3** Colocalization of N-glycosylation-deficient hACE2 variants with ER. (A) Expression of the N-glycosylation hACE2 mutants was analyzed by Western blotting using anti-FLAG antibody and GAPDH as a loading control. Densitometry of hACE2 bands shown below the (Continued on next page)

mutant on the cell surface was decreased compared with that of wild-type hACE2 (Fig. 4C). Additionally, KIF treatment did not reduce the cell surface expression of both hACE2 and pACE2 (Fig. 4D), which is consistent with the immunofluorescence data shown above (Fig. 2C). To further verify that N-glycosylation is required for an adequate cell surface expression of hACE2, we quantified the plasma membrane levels of both wild-type hACE2 and hACE2\* mutant by fluorescence-activated cell sorter (FACS). As shown in Fig. 4E, the cell surface expression of the N-glycosylation deficient mutant is drastically reduced compared with that of wild-type hACE2, which agrees with the results of the cell surface biotinylation experiments. Altogether, these data demonstrate that ACE2 N-deglycosylation results in a pronounced decrease of cell surface expression, which is in agreement with the findings shown in the previous section.

**N-glycosylation is not necessary for the carboxypeptidase activity of ACE2.** To test the impact of N-glycosylation on the folding of ACE2 receptor, we determined the carboxypeptidase activity of both nonglycosylated hACE2 and pACE2, generated by either TM treatment of cells or mutagenesis. To directly analyze the carboxypeptidase activity of ACE2 proteins, we tested the ability of immunoprecipitated ACE2 variants (Fig. 5A and B) to hydrolyze a synthetic peptide substrate. The ACE2 variants described in the Western blot to the right of each graph were incubated with a fluorophore-labeled substrate. As shown in Figure 5A and B, the constructs lacking glycosylation did not lose carboxypeptidase activity compared to the wild type. These results show that N-glycosylation is not required for ACE2 protease activity and also suggest that the N-glycosylation-deficient ACE2 variants are in a native conformational state.

**N-glycosylation inhibition of ACE2 receptor and/or SARS-CoV-2/SARS-CoV-2 S protein does not disrupt S-ACE2 association.** The ACE2 receptor is extensively glycosylated, bearing high-mannose, hybrid, or complex carbohydrates distributed among its 7 N-glycosylation sites (Fig. 1A) (32–35). Several functions have been proposed for these N-glycans, including a direct modulation of spike-ACE2 binding (34–36). Recent studies investigated the role of ACE2 N-glycosylation in the interaction with SARS-CoV-2 S protein (37, 38). To this end, they generated different hACE2 glycoforms. Specifically, the N-linked sugars displayed by hACE2 were modified genetically or enzymatically (37, 38). However, the effect of a whole blocking of hACE2 N-glycosylation, by removing all the N-glycans from ACE2, on the binding to S protein was not investigated (37, 38). To assess the importance of N-glycosylation on ACE2-S binding, we analyzed the biochemical ability of N-glycosylation-deficient ACE2 variants containing a FLAG tag to interact with untagged S protein. For this purpose, we first transfected cells independently with plasmids expressing either hACE2 or S. Cells were lysed, and cell lysates containing FLAG-tagged hACE2 and untagged S protein were mixed. After precipitation with anti-FLAG beads, the eluted proteins by the FLAG peptide were separated by SDS-PAGE gels and analyzed by Western blotting using antibodies directed against the FLAG tag and the S protein. The SARS-CoV-2 S protein was efficiently coprecipitated by the anti-FLAG antibody, which is consistent with previous reports that demonstrated that hACE2 interacts with SARS-CoV-2 S protein (Fig. 6A) (4, 16–18, 26, 55–58). Similar results were obtained when we used pACE2 as the bait to pull

### FIG 3 Legend (Continued)

immunoblots are normalized to the loading control, GAPDH. Fold changes are shown relative to empty vector (pCDNA3.1), and results are means  $\pm$  SD values from three independent experiments (\*,  $P < 0.05$ ; NS, not significant). (B) Semiconfluent monolayers of HEK 293T cells grown on coverslips were transfected with the indicated hACE2 mutants. All cells were fixed and immunostained as in Figure 2. (C) Quantification of colocalization of ACE2 variants and ER was performed as described in Figure 2. Pearson's correlation coefficient (PCC) values between the ACE2 staining and intracellular endoplasmic reticulum marker are shown on the plot. Values are means  $\pm$  SD from one representative experiment performed in triplicate. \*\*\*,  $P < 0.0005$  (as determined by two-tailed Student's *t* test) compared with the wild-type hACE2. Similar results were obtained in three separate experiments and representative data are shown. (D) Semiconfluent monolayers of HEK 293T cells grown on coverslips were transfected with hACE2-, hACE2\*-, or pACE2-expressing plasmids, and the cells were incubated with TM (1  $\mu$ g/ml) (+TM) dissolved in DMSO or DMSO only (+DMSO) for 16 h, fixed, and stained using anti-FLAG antibody and then with Alexa 594-conjugated goat anti-mouse IgG (red). ER was visualized by staining cells with calnexin antibody, followed by Alexa 488-conjugated goat anti-rabbit IgG (green). Nuclei were counterstained with DAPI (blue). Similar results were obtained in three separate experiments and representative data are shown.

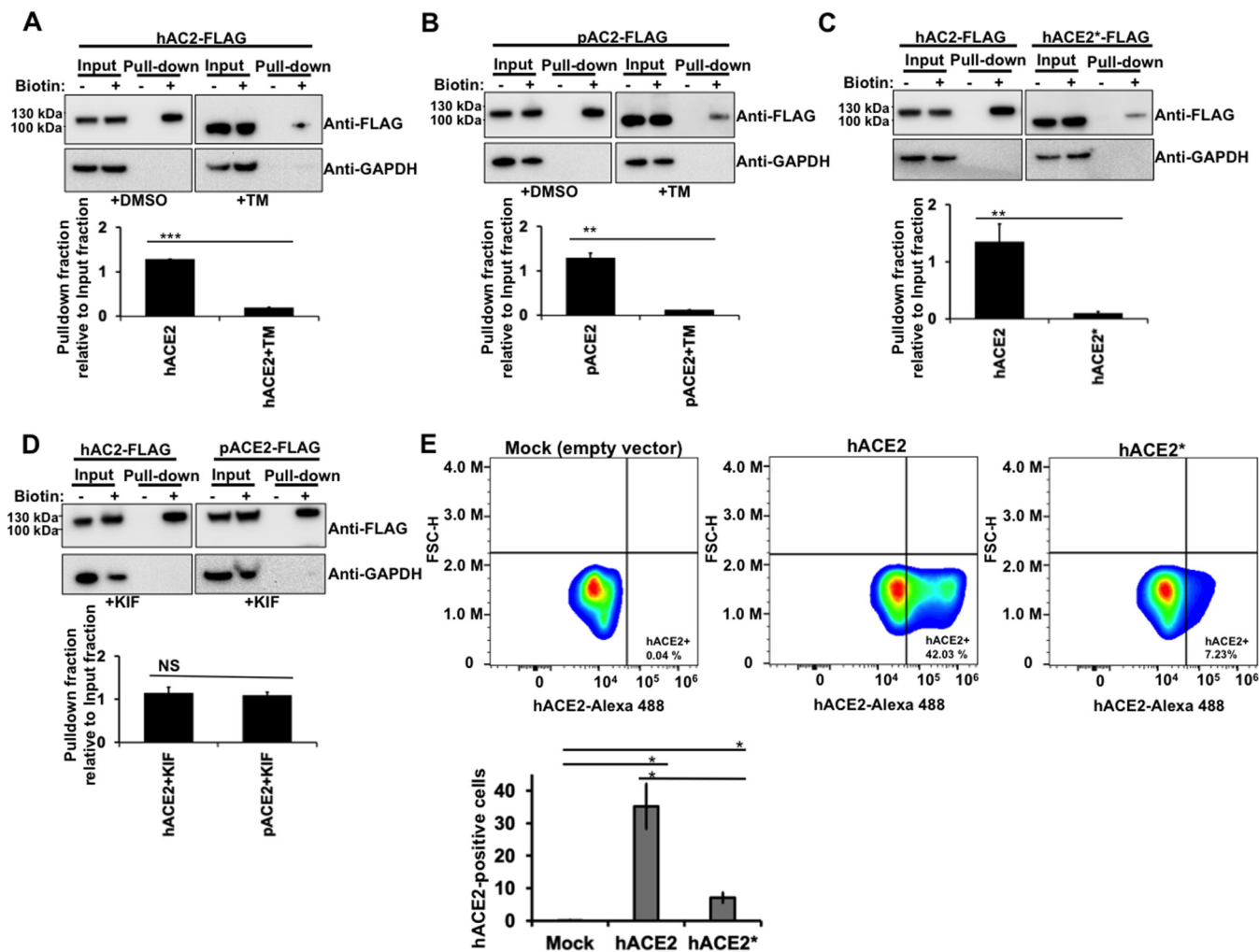


**FIG 4** N-glycosylation inhibition and cell surface expression of ACE2. (A through D) HEK 293T cells were transiently transfected for 24 h with the indicated FLAG-tagged ACE2 constructs. Where stated, transfected cells were incubated with either TM (1  $\mu$ g/ml) or KIF (5  $\mu$ g/ml) for 16 h before biotin labeling. Cells were treated with (+) or without (–) biotin to label surface protein for 1 h at 4°C. After neutravidin agarose pull-down, proteins were immunoblotted with anti-FLAG antibody. GAPDH was used as the control to assess the purity of biotinylated plasma membrane fractions. The amount of pull-down fraction (Biotin+) relative to input fraction (Biotin+) for three independent experiments with standard deviations is shown. \*\*,  $P < 0.005$ ; \*\*\*,  $P < 0.0005$ ; NS, not significant. (E) HEK 293T cells were transfected with either hACE2\*– or hACE2-expressing plasmid. The percentage of hACE2-positive cells was measured at 24 h posttransfection by FACS. Results are means  $\pm$  SD values from three independent experiments (\*,  $P < 0.05$ ). Representative data sets are shown for hACE2 and hACE2\* surface staining (upper panels). FSC-H, forward scatter height.

down the S protein (Fig. 6A). This finding is in agreement with the observation that expression of pACE2 on nonpermissive cells to SARS-CoV-2 infection enables viral entry and infection (4, 40). Colocalization experiments in cotransfected cells confirmed the interaction of both hACE2 and pACE2 with SARS-CoV-2 S protein (Fig. 6B). Next, we tested the ability of N-glycosylation-deficient ACE2 variants, generated by either TM treatment or mutagenesis, to bind S by performing similar methods. As shown in Figure 7A and B, the nonglycosylated variants of hACE2 and pACE2, generated after TM treatment, were able to interact with S protein. Similarly, the N-glycosylation-defective ACE2 mutant showed association with S protein (Fig. 7C). These results indicate that N-glycosylation is not required for the ability of ACE2 to bind SARS-CoV-2 S protein. Furthermore, a nonglycosylated variant of S generated after TM treatment was able to interact with ACE2, suggesting that N-glycosylation of SARS-CoV-2 S protein is not required for its capacity to bind ACE2 receptor (Fig. 7A and B). It is important to point out that the expression of the nonglycosylated S variant was detected in the pull-down assay only when ACE2 was used as bait (Fig. 7A and B), suggesting that the blocking of N-glycosylation might affect the stability or expression of the S protein. To

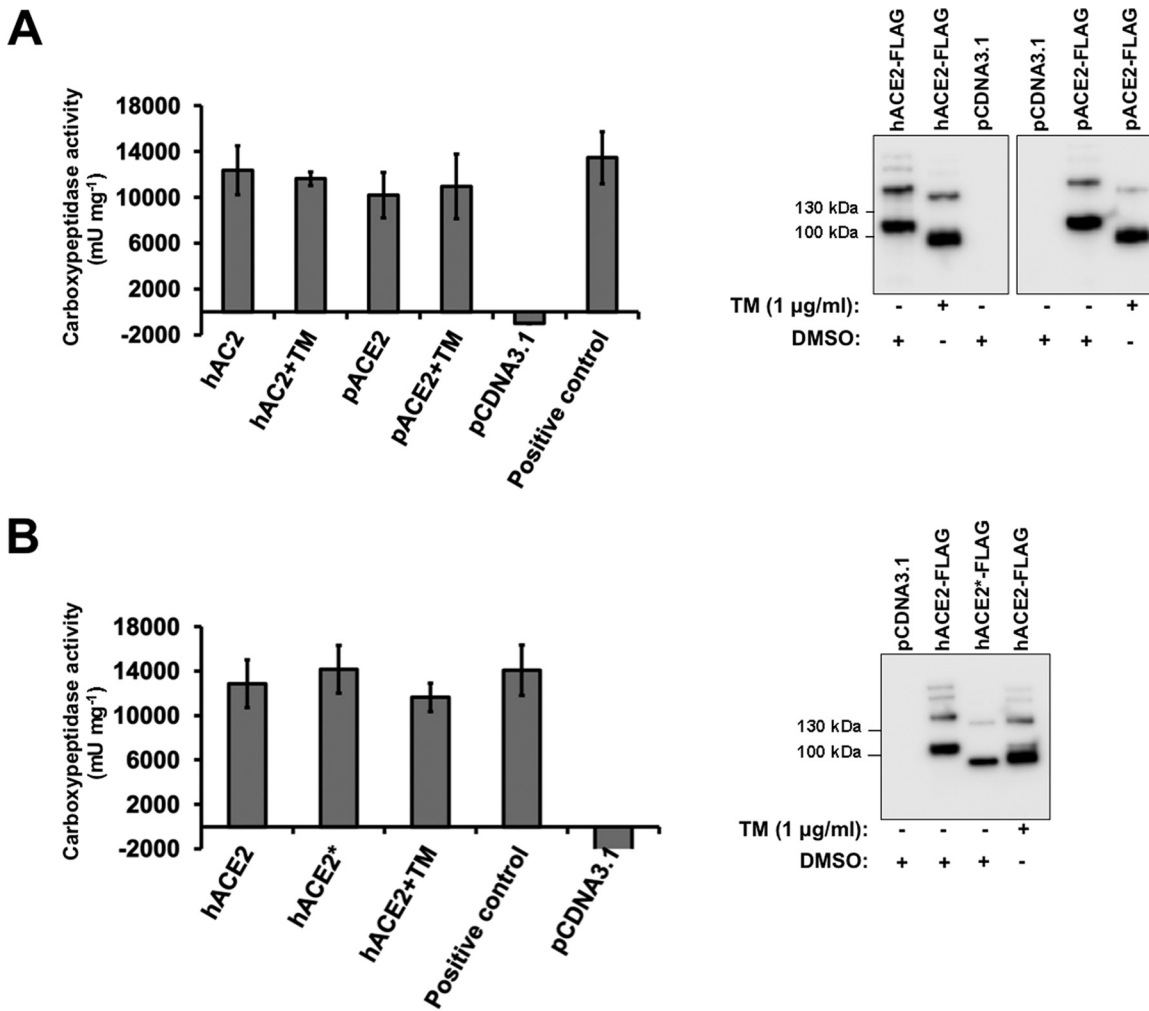


**FIG 5** ACE2 carboxypeptidase activity in the absence of glycosylation. (A) Plot showing the results of carboxypeptidase assays using the indicated immunoprecipitated FLAG-tagged ACE2 variants. A representative Western blot with an anti-FLAG antibody that detects immunoprecipitated ACE2 variants is shown on the right. (B) The same as panel A, but showing the results of carboxypeptidase assays using the immunoprecipitated FLAG-tagged hACE2\* mutant. A representative Western blot with an anti-FLAG antibody that detects immunoprecipitated hACE2 variants is shown on the right. Results are means  $\pm$  SD values from three independent experiments.

confirm that the TM treatment generated an N-glycosylation-defective S variant, untreated S-containing lysates were digested with PNGase F. As expected, both treatments created S protein bands of similar sizes (Fig. 7D). Consistently, N-deglycosylation of both ACE2 and S protein by mutagenesis or TM treatment, respectively, did not disrupt their interaction (Fig. 7E). Additional colocalization data further confirmed the association between the N-glycosylation-deficient ACE2 variants and the spike protein (Fig. 7F and G). Finally, we explored the ability of SARS-CoV S protein to bind nonglycosylated ACE2 variants. As shown in Figure 8A and D, N-glycosylation-defective ACE2 variants from human and pig were capable to bind SARS-CoV S protein, which agrees with a previous study that showed that modifications of the N-linked glycan structure of hACE2 did not affect its binding to the S protein (59). Colocalization results verified the S-ACE2 association (Fig. 8B and F). Moreover, a nonglycosylated S variant, generated by TM treatment, was able to interact with ACE2 receptors (Fig. 8A and D). Similar to SARS-CoV-2 S protein, the expression of the nonglycosylated S variant was detected in the pulldown assay only when ACE2 was used as bait (Fig. 8A and D), suggesting that the blocking of N-glycosylation might affect the stability or expression of the S protein. In addition, digestion of untreated S-containing lysates with PNGase F affirmed

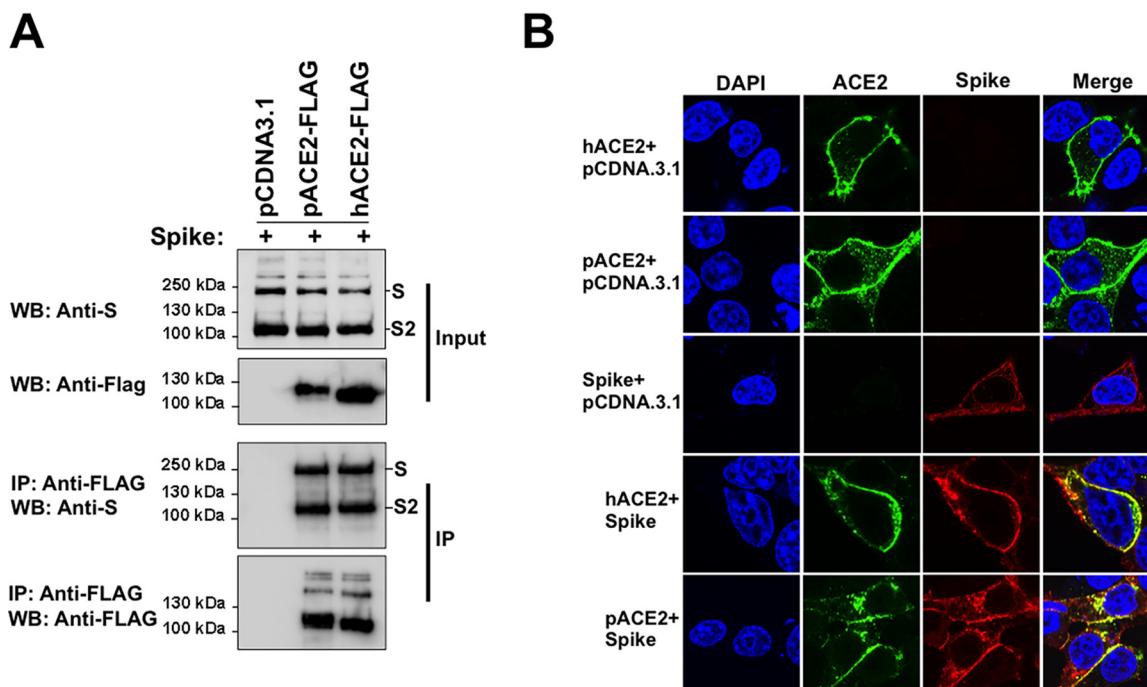


**FIG 6** Coimmunoprecipitation assays and colocalization experiments to analyze ACE2-spike interactions. (A) HEK 293T cells were independently transfected with vectors expressing the indicated FLAG-tagged hACE2 or pACE2 proteins. Other cells were transfected with an S-expressing vector. Cells expressing ACE2 variants or S protein were lysed at 24 h posttransfection. The cell lysates were mixed in a 1:1 ratio and incubated with anti-FLAG beads. To control for background binding of S protein to anti-FLAG beads, we performed similar experiments with HEK 293T cells that were independently transfected with an S-expressing plasmid or an empty pCDNA3.1 vector. The amount of untagged and FLAG-tagged proteins in the lysates (Input) and immunoprecipitates (IP) was analyzed by Western blotting with anti-S and anti-FLAG antibodies. WB, Western blot; IP, immunoprecipitation. Similar results were obtained in three independent experiments and representative data are shown. (B) Cellular colocalization of ACE2 variants and S protein. Cells were cotransfected with ACE2-expressing plasmids and an S-expressing vector. After 24 h, cells were fixed and immunostained using anti-FLAG antibody followed by Alexa 488-conjugated goat anti-rabbit IgG (green). The S protein was visualized using anti-S monoclonal antibody, followed by Alexa 594-goat anti-mouse IgG (red). Nuclei were counterstained with DAPI (blue). Similar results were obtained in three separate experiments and representative data are shown.

that TM treatment produced an N-glycosylation-defective S variant (Fig. 8C). Consistently, the N-deglycosylation of both ACE2 and S protein by mutagenesis, or TM treatment of cells, respectively, did not disrupt their interaction (Fig. 8E). Overall, these findings indicated that N-glycosylation is not required for the ability of ACE2 to bind either SARS-CoV S or SARS-CoV-2 S protein.

**hACE2 N-glycosylation impairment decreases cell-to-cell fusion mediated by SARS-CoV S protein but not that mediated by SARS-CoV-2 S protein.** Both furin or type II membrane serine proteases (TMPRSS)-mediated cleavage can trigger the fusogenic ability of both SARS-CoV-2 S and SARS-CoV S proteins, inducing receptor-dependent syncytial formation (25–27, 60–64). To investigate the effect of ACE2 N-glycosylation of either SARS-CoV-2 or SARS-CoV S-glycoprotein-driven cell-to-cell fusion, we performed a widely adopted S-mediated cell-cell fusion assay (61, 65). The assay is based on the expression of green fluorescent protein (GFP) in one of the effector cells. Fusion of the cells is evident by the movement of GFP into the non-GFP-expressing partner cell, resulting in the formation of multinucleated large green cells. For this experiment, we used 293T cells that expressed either SARS-CoV-2 or SARS-CoV S protein and GFP (293T/GFP/spike) as the effector cells and 293T cells expressing either wild-type ACE2 or an N-glycosylation-defective ACE2 variant as the target cells (293T/hACE2, 293T/hACE2\*). Cell surface biotinylation experiments showed similar cell surface expression levels of S proteins from both coronaviruses in the effector cells (Fig. 9B). For the SARS-CoV S-mediated cell-cell fusion assay, effector cells were detached with trypsin and overlaid on target cells coexpressing ACE2 variants and TMPRSS2 to facilitate the fusion mediated by the S protein. In the case of SARS-CoV-2 S

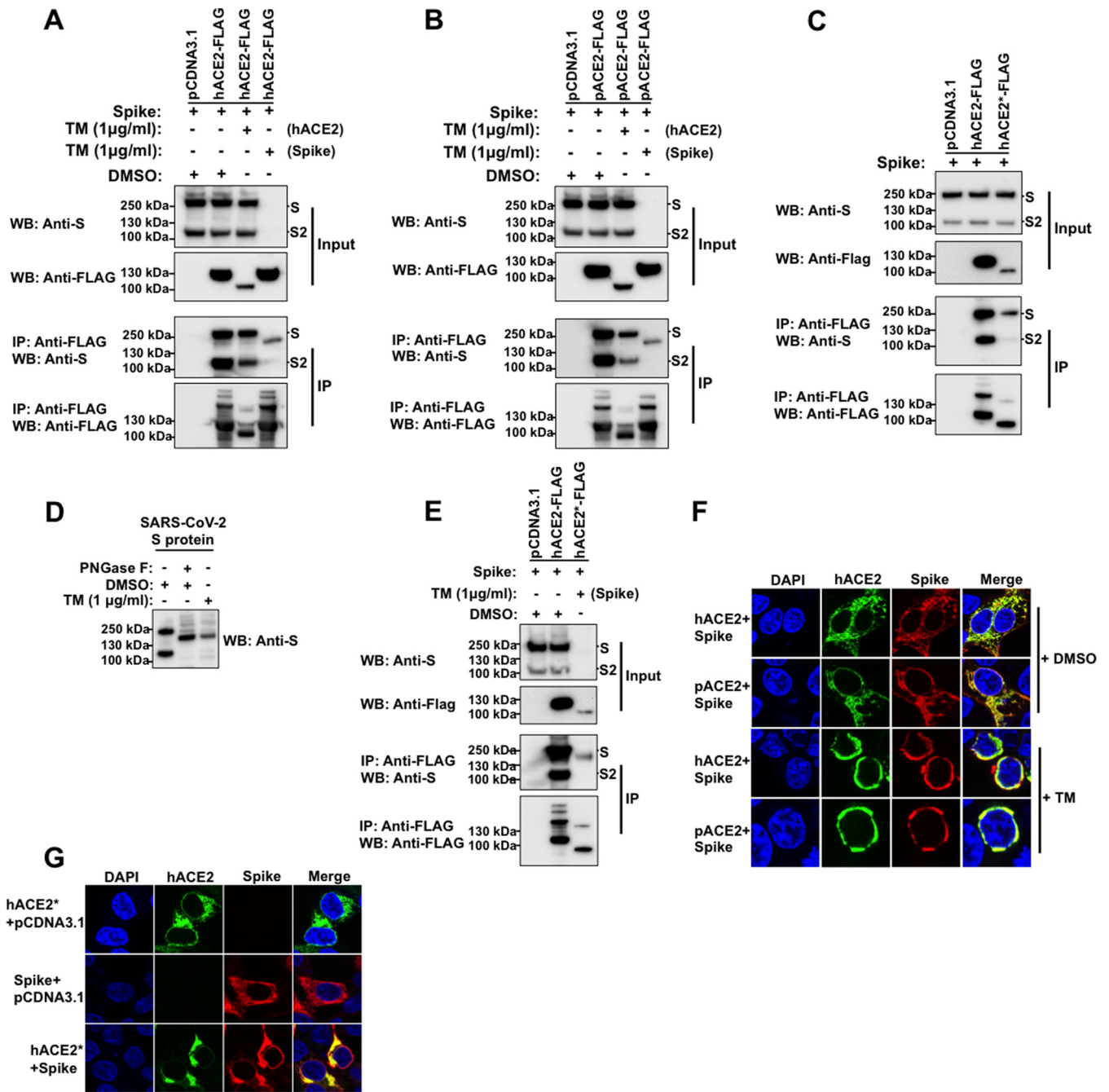


**FIG 7** Role of N-glycosylation in ACE2/S colocalization and binding. (A through C) The same Western blotting and immunoprecipitation experiments as those in Figure 6A were repeated but in the presence of TM (1 µg/ml). Cells were lysed 24 h after transfection. (D) 293T cells were transfected with a plasmid expressing SARS-CoV-2 S protein and treated with TM (1 µg/ml). Sixteen hours posttreatment, the S protein was precipitated by using ACE2 as bait (lane 3), as indicated in Figure 6. Cell lysates were also digested with PNGase F (lane 2). All the samples were analyzed by Western blotting using anti-S monoclonal antibody. (E) The same as panel C, but both S and ACE2 protein were deglycosylated. (F and G) Cells were cotransfected with ACE2-expressing plasmids and an S-expressing vector. Cells were either untreated (+DMSO) or incubated with TM (1 µg/ml) (+TM) dissolved in DMSO for 16 h. All cells were fixed and immunostained using anti-FLAG antibody and then with Alexa 488-goat anti-rabbit IgG (green). S protein was visualized by immunostaining with anti-S monoclonal antibody, followed by Alexa 594-goat anti-mouse IgG (red). Nuclei were counterstained with DAPI (blue). Similar results were obtained in three separate experiments and representative data are shown.

protein-triggered membrane fusion assay, cells were detached with 1 mM EDTA and overlaid on target cells. Syncytia formation was assessed by fluorescence microscopy. After effector and target cells were cocultured for 24 h, the formation of big syncytia was observed in wild-type hACE2-expressing target cells. This occurred when either SARS-CoV or SARS-CoV2 S protein was used. (Fig. 9A and C). No fusion was observed

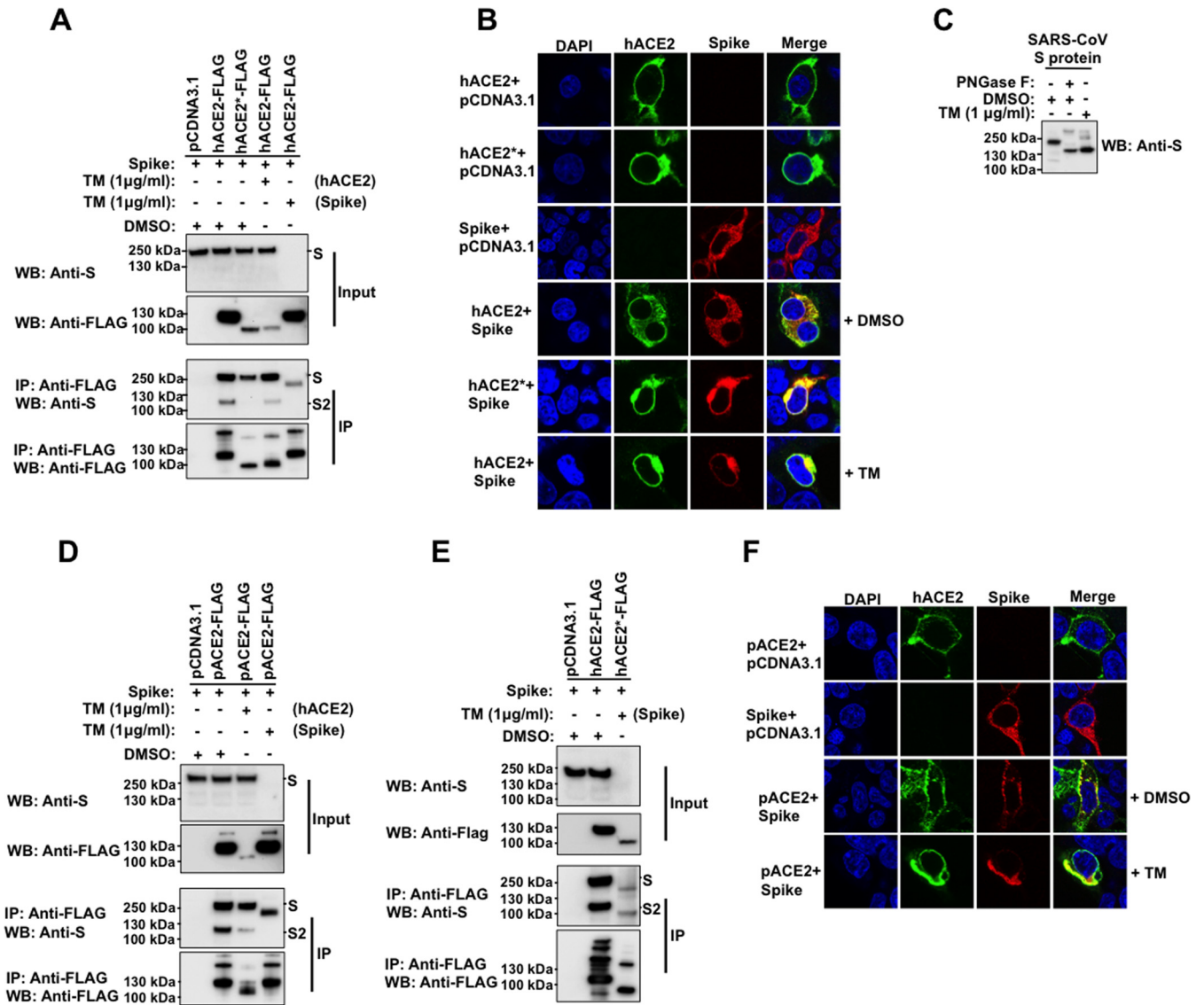


**FIG 8** Blocking of N-glycosylation of SARS-CoV S protein and/or ACE2 does not disrupt their binding and cellular colocalization. (A) HEK 293T cells were independently transfected with the following vectors: an empty pCDNA3.1 vector, a vector expressing either hACE2 or hACE2\* protein with a FLAG epitope tag, or an untagged S-expressing vector, followed by TM (1  $\mu$ g/ml) treatment for 16 h. Cytosolic extracts were prepared separately at 24 h posttransfection, mixed in a 1:1 ratio, and used for immunoprecipitation with an anti-FLAG antibody. The amount of untagged and FLAG-tagged proteins in the lysates (Input) and immunoprecipitates (IP) was analyzed by Western blotting with anti-S and anti-FLAG antibodies. WB, Western blot; IP, immunoprecipitation. (B) HEK 293T cells were cotransfected with either hACE2- or hACE2\*-expressing plasmids and an empty pCDNA3.1 plasmid or an S-expressing vector for 24 h. Cells were either untreated (+DMSO) or incubated with TM (1  $\mu$ g/ml) (+TM) dissolved in DMSO for 16 h. Cells were fixed and immunostained as described in Figure 7. (C) HEK 293T cells were transfected with a plasmid expressing S protein and treated with TM (1  $\mu$ g/ml). Sixteen h posttreatment, the S protein was precipitated by using hACE2 as bait (lane 3), as described above. Cell lysates were also digested with PNGase F (lane 2). All the samples were analyzed by Western blotting using anti-S monoclonal antibody. (D) same as panel A, but the HEK 293T cells were transfected with a pACE2-expressing plasmid. The procedure for the coprecipitation is also the same as that described in panel A. (E) Same as panel A, but both S and hACE2 protein are deglycosylated. (F) Same as panel B, but the HEK 293T cells were transfected with a pACE2-expressing plasmid. The immunofluorescence analysis was also performed as indicated in panel B. Similar results were obtained in three independent experiments and representative data are shown.

for GFP-expressing effector cells without S expression or target cells without ACE2 expression (Fig. 9A and C), which confirms that S receptor engagement is required for the S-mediated viral fusion. Subsequently, we analyzed the fusogenic capacity of SARS-CoV-2/SARS-CoV S protein in target cells expressing the N-glycosylation-deficient hACE2 mutant. As shown in Fig. 9A and C, SARS-CoV S protein lost the ability to mediate cell-cell fusion when hACE2 N-glycosylation was impaired. This finding is consistent with the fact that the N-glycosylation-defective hACE2 variant is less expressed in the cell surface compared to the wild-type hACE2, which would indirectly reduce the

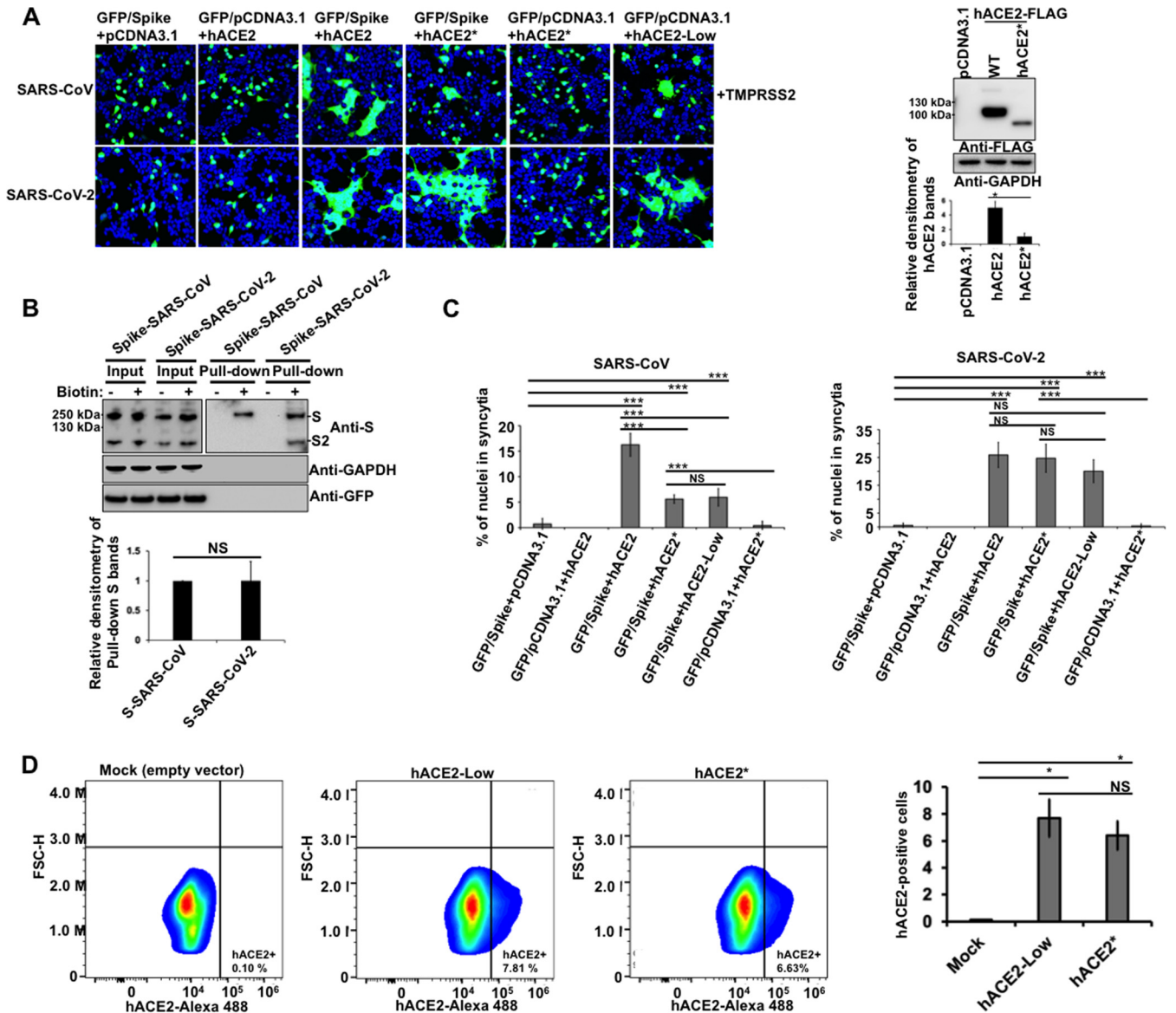


**FIG 9** Effect of hACE2 N-glycosylation on SARS-CoV S and SARS-CoV-2 S protein fusion activity. (A) HEK 293T effector cells were cotransfected with a GFP-expressing plasmid along with one of the following plasmids: a plasmid expressing SARS-CoV-2 S protein, a plasmid expressing SARS-CoV S protein, or an empty pCDNA3.1 plasmid. At 24 h posttransfection, cells were detached and cocultured with HEK 293T target cells coexpressing either hACE2 or hACE2\* and TMPRSS2 for 24 h. Target cells transfected with an empty plasmid were included as the negative control. Representative results are shown. A Western blot showing expression of hACE2 and hACE2\* proteins is shown on the right. GAPDH was used as a loading control. Densitometry of hACE2 bands shown below the immunoblots is normalized to the loading control, GAPDH. Fold changes are shown relative to empty vector (pCDNA3.1) and results are means  $\pm$  SD values from three independent experiments (\*,  $P < 0.05$ ; NS, not significant). (B) Biotinylation of effectors cells coexpressing GFP and SARS-CoV-2 S protein or SARS-CoV S protein. Cells were treated with (+) or without (-) biotin to label surface protein for 1 h at 4°C. After neutravidin agarose pulldown, proteins were immunoblotted with anti-S antibody. GAPDH and GFP were used as controls to assess the purity of biotinylated plasma membrane fractions. Densitometry analysis of the pulldown S bands is shown; bands were normalized to the SARS-CoV S protein and data are mean values of three independent experiments (NS, not significant). (C) Quantitative representation of syncytia shown in panel A. Results are means  $\pm$  SD values from three independent experiments. \*\*\*,  $P < 0.0005$ ; NS, not significant with respect to the negative controls, hACE2\*, and hACE2-Low. (D) HEK 293T cells were transfected with either hACE2\* or hACE2-expressing plasmids. To normalize cell surface expression of both hACE2 proteins, the DNA amount of hACE2-expressing plasmid used for transfection was reduced 4.5 times. The percentage of hACE2-positive cells was measured at 24 h posttransfection by FACS. Results are means  $\pm$  SD values from three independent experiments (\*,  $P < 0.05$ ). Representative data sets are shown for hACE2 and hACE2\* surface staining (upper panels). FSC-H, forward scatter height.

fusogenic capacity of the S protein. On the contrary, SARS-CoV-2 S protein did not lose the ability to mediate the cell-cell fusion under the same conditions. No statistically significant differences were observed in syncytia formation comparing nonglycosylated with wild-type hACE2 (Fig. 9A and C). Thus, in contrast to SARS-CoV S protein, SARS-CoV-2 S protein was much more effective in mediating cell-cell fusion into target cells

expressing an N-glycosylation-deficient hACE2 variant. To analyze whether the loss of capacity of the SARS-CoV S protein to mediate cell-cell fusion was due exclusively to the low membrane levels of hACE2\*, we decided to normalize the cell surface expression of both hACE2 and hACE2\* proteins by reducing the plasma membrane hACE2 levels (for clarity, hACE2 expressed at cell surface levels similar to those of hACE2\* is herein referred to as hACE2-Low). To this end, we decreased the amount of the hACE2-expressing plasmid during transfection, and then we quantified the cell surface expression of both hACE2 and hACE2\* receptors by FACS. As shown in Figure 9D, this experimental approach resulted in both proteins being expressed at similar levels at the cell surface. Next, we tested the ability of S protein of both coronaviruses to induce cell-cell fusion in cells expressing hACE2-Low. Our investigations revealed that the capacity of SARS-CoV S protein to mediate cell-cell fusion diminished when the cell surface expression of hACE2 was reduced to levels similar to those of hACE2\* (Fig. 9A and C). In contrast, SARS-CoV-2 S protein was much more effective than SARS-CoV S protein in mediating cell-cell fusion into target cells expressing hACE2-Low (Fig. 9A and C). These results confirm that the loss of the ability of SARS-CoV S protein to mediate cell-to-cell fusion when hACE2 N-glycosylation was impaired is due to the lack of available cell surface hACE2. Overall, these findings suggest that the SARS-CoV-2 S protein has a higher capacity to mediate membrane fusion than that of the SARS-CoV S protein. This is in agreement with previous reports that show that the increased ability to mediate cell-cell fusion of the SARS-CoV-2 S protein is likely due to the presence of a furin cleavage site in its sequence (27, 61, 65).

**Effect of hACE2 N-glycosylation inhibition on SARS-CoV/SARS-CoV-2 viral entry.** Based on our previous findings that demonstrate that N-glycosylation is required for proper ACE2 cell surface expression, we hypothesized that viral entry of SARS-CoV-2 might be reduced in cells expressing a nonglycosylated variant of hACE2. To test this possibility, we analyzed the impact of hACE2 N-glycosylation on viral entry. For this purpose, we determined whether GFP-expressing SARS-CoV-2 S pseudotyped viruses were able to transduce 293T cells expressing wild-type hACE2 or an N-glycosylation-deficient ACE2 variant (hACE2\*). The hACE2 proteins were transiently expressed (Fig. 10A), and then the ability of hACE2 receptors to allow SARS-CoV-2 S pseudovirions entry was tested. Vesicular stomatitis virus (VSV-G) pseudotyped viruses were used as a positive control. As expected, all transfected cells were effectively transduced by VSV-G pseudotyped viruses (Fig. 10B and C). Compared to transduction of cells transfected with empty plasmid (mock control) that were not susceptible to viral entry of SARS-CoV-2 S pseudotyped viruses, transduction of wild-type hACE2-expressing cells with SARS-CoV-2 pseudoviral particles showed more GFP-positive cells. This observation is consistent with previous findings that demonstrated that hACE2 is the receptor for SARS-CoV-2 (4, 16, 17, 56). In contrast, the viral entry of SARS-CoV-2 S pseudotyped viruses in nonglycosylable ACE2-expressing cells was reduced compared to that in hACE2-expressing cells (Fig. 10B and C), suggesting that ACE2 needs to be N-glycosylated to support viral entry. Similarly, viral entry of SARS-CoV S pseudotyped viruses was also reduced in cells expressing an N-glycosylation-deficient variant (Fig. 10B and C). These findings indicated that hACE2 N-glycosylation is required to allow an efficient viral entry of both SARS-CoV-2 and SARS-CoV, which confirms our previous results that showed that N-glycosylation is a prerequisite for the proper cell surface expression of hACE2. To verify that the decrease of viral entry of SARS-CoV/SARS-CoV-2 S pseudotyped viruses in nonglycosylable ACE2-expressing cells is due exclusively to the low membrane levels of hACE2\*, we analyzed the viral entry in hACE2-Low-expressing cells. As shown in Fig. 10B and C, the viral entry for both coronaviruses was compromised when the cell surface expression of hACE2 was reduced to levels similar to those of hACE2\*. These findings confirm that the decrease in viral entry of both coronaviruses, when hACE2 N-glycosylation was impaired, is due to the lack of available cell surface hACE2.

**N-glycosylation is not important for hACE2 protein stability.** Our data showed that the levels of wild-type hACE2 protein were higher than those of the N-

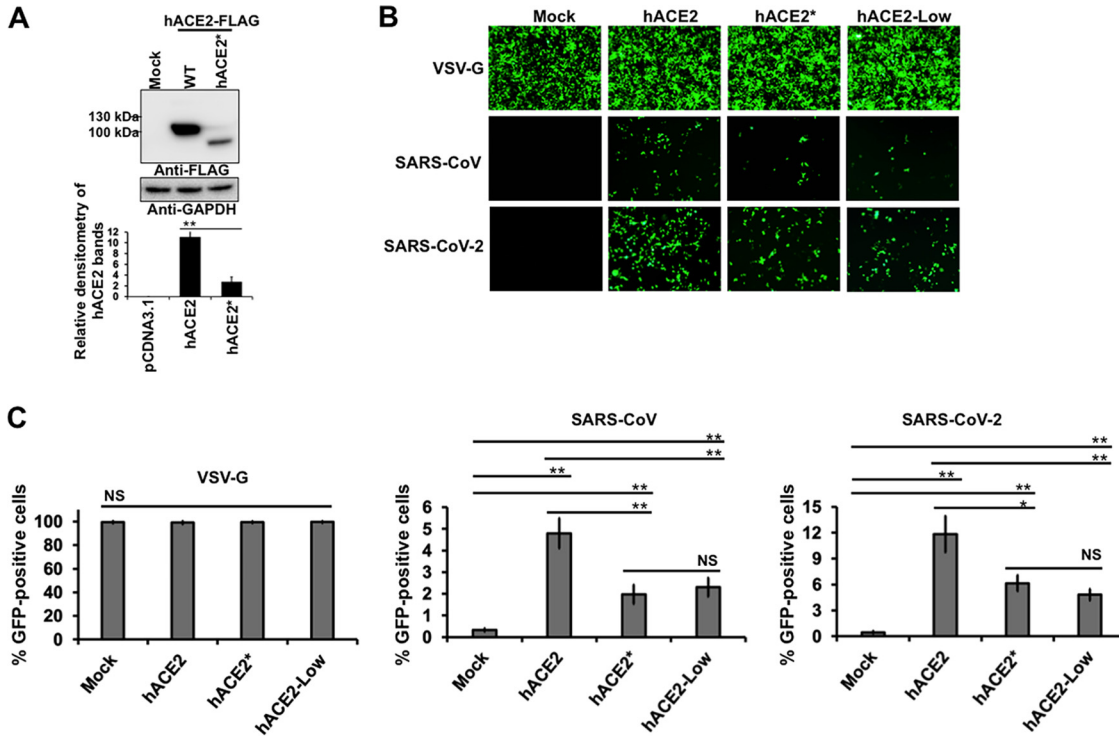


**FIG 10** Contribution of ACE2 N-glycosylation to viral entry of SARS-CoV/SARS-CoV-2 S pseudotyped viruses. (A) HEK 293T cells were transiently transfected with plasmids expressing hACE2 or hACE2\* proteins, and their expression levels were analyzed by Western blotting using anti-FLAG and anti-GAPDH antibodies. Densitometry of hACE2 bands shown below the immunoblots are normalized to the loading control GAPDH. Fold changes are shown relative to empty vector (pCDNA3.1) and results are means ± SD values from three independent experiments (\*\*,  $P < 0.005$ ; NS, not significant). (B) Representative fluorescence images of HEK 293T cells expressing wild-type hACE2 or hACE2\* after infection with equalized amounts of GFP-expressing SARS-CoV, SARS-CoV-2, or VSV-G pseudotyped viruses. (C) The percentage of GFP-positive cells was measured at 72 h postinfection by FACS. Wild-type VSV-G was used as a positive control. Results are means ± SD values from three independent experiments. \*,  $P < 0.05$ ; \*\*,  $P < 0.005$ ; NS, not significant.

glycosylation-deficient ACE2 mutant, suggesting that N-glycosylation inhibition might affect the stability or expression of the ACE2 receptor. Since N-glycosylation plays an important role in protein stability by protection against proteolysis (66–68), we investigated whether hACE2 protein stability is affected by the presence of its N-linked glycan motifs. Cycloheximide (CHX), an inhibitor of protein synthesis, was used to analyze the turnover rates of the hACE2 variants. We found that after up to 10 h of drug treatment, hACE2 and hACE\* levels did not change, suggesting that N-glycosylation is not implicated in hACE2 stability and is not absolutely required for correct folding (Fig. 11).

**DISCUSSION**

Overall, the study presented here shows the importance of ACE2 N-linked glycosylation in cell membrane expression and protease activity as well as in various roles of ACE2, including binding to SARS-CoV-2/SARS-CoV-2 S protein, cell-cell fusion mediated by SARS-CoV/SARS-CoV-2 S protein, and viral entry of SARS-CoV-2/SARS-CoV-2 S pseudotyped viruses. From these studies, we have learned the following: (i) N-glycosylation is a major determinant for the biosynthesis and proper cell surface expression of ACE2, (ii) ACE2 N-glycosylation is not required for its carboxypeptidase activity, (iii) association of SARS-CoV-2/SARS-CoV-2 S protein with ACE2 is not disrupted by N-glycosylation inhibition of ACE2 receptors or the viral proteins, (iv) impairment of hACE2 N-glycosylation affects cell-cell fusion mediated by SARS-CoV S protein but not the membrane fusion induced by SARS-CoV-2 S protein, and (v) hACE2 N-glycosylation is indirectly required for an efficient viral entry of the SARS-CoV/SARS-CoV-2 S pseudotyped viruses.

In agreement with previous studies (32–36), we verified, by digestion with

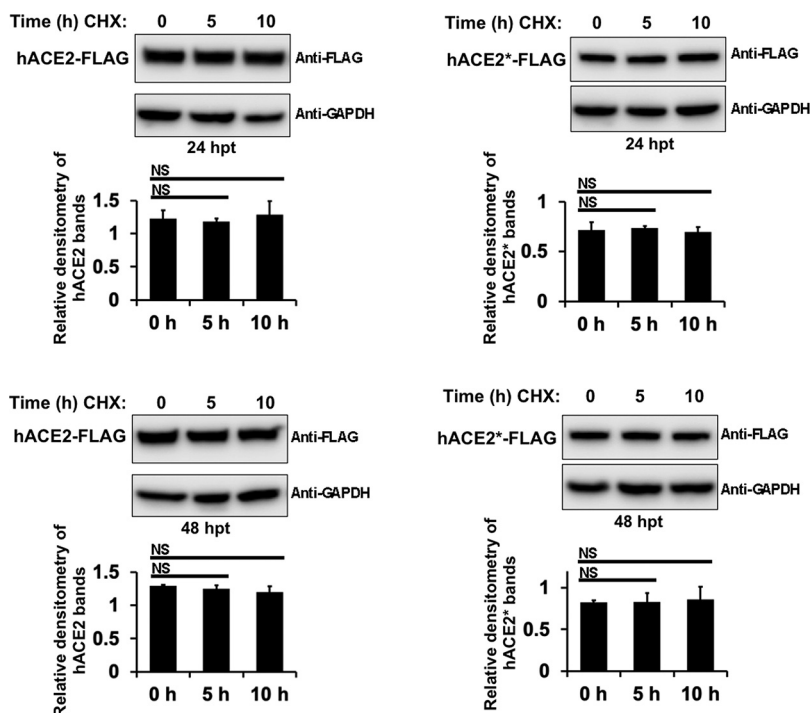


**FIG 11** Glycosylation is not important for hACE2 protein stability. HEK 293T cells were transiently transfected with hACE2- or hACE2\*-expressing plasmids for 24 to 48 h. Cells were then treated with 100  $\mu$ g/ml of cycloheximide (CHX) for a period of 10 h. At the indicated times after the beginning of the CHX treatment, cells were lysed. Cell lysates were analyzed with Western blotting and probed with antibodies directed against either the FLAG epitope tag or GAPDH. Densitometry of ACE2 bands shown below the immunoblots are normalized to the loading control GAPDH. Fold changes are shown relative to 0 h and data are mean values of three independent experiments (NS, not significant).

glycosidases and by treatment with inhibitors that interfere at different stages of N-glycosylation biosynthesis, that hACE2 is N-linked glycosylated. Digestion with endo H confirmed a small presence of high-mannose/hybrid type glycans at the hACE2 receptor. This finding is consistent with previous glycomic and glycoproteomic analysis that found that complex-type glycans were much more abundant than high-mannose/hybrid type glycans across all N-glycosylation sites of hACE2 (34, 35). By using the same methods, we also found that pACE2, which showed four similar N-glycosylation sites with human ACE2 (Fig. 1A), displays an N-glycosylation pattern similar to that of its homologous hACE2. These results suggest the presence of N-linked glycans in ACE2 receptors across different related species.

A large body of evidence describes important roles for N-glycosylation in protein stability and in cell surface expression of biomolecules (46, 47, 69–72). Our findings demonstrate that the complete deglycosylation of ACE2 by site-directed mutagenesis or TM treatment results in a significant decrease in cell surface expression of the ACE2 receptor (Fig. 2 and 3). Reduced surface expression is the consequence of reduced protein expression (Fig. 1 and 4) along with increased retention in the ER (Fig. 2 and 3). As shown in Figure 3B, the loss of five N-glycosylation sites, represented by N90Q/N322Q/N546Q/N533Q/N103Q, is sufficient to retain ACE2 in the ER. Colocalization studies showed that deglycosylated ACE2 was localized predominantly to the ER and not in the Golgi apparatus, suggesting that N-glycosylation is important for the biosynthetic processing from the ER. In the absence of N-glycans, Golgi apparatus processing is prevented, blocking the secretory pathway through the Golgi apparatus. Incubation of cells with KIF resulted in the loss of complex glycosylation of ACE2 but did not result in retention in the ER. This result shows that complex N-glycosylation is not required for surface expression of ACE2 (Fig. 2 and 4), allowing the surface expression of ACE2

lacking complex sugars. This finding is consistent with a previous work that showed that inhibition of ER glucosidases with iminosugars did not affect ACE2 expression on the cell surface (59).

Another potential role for N-glycosylation is the effect on the interaction between ACE2 and the S protein. There are several examples for the requirement of N-glycosylation in the formation of protein-protein interactions. For instance, N-glycosylation of the vasopressin V1a receptor is needed for optimal receptor-ligand binding (73) and N-glycosylation of P2Y12 receptor is necessary to trigger proper downstream Gi-mediated signaling (74). In contrast, N-glycosylation is not required for the receptor functions of angiotensin II type-1 receptor (75), histamine H2 receptor (76), and the orphan G protein-coupled receptor Gpr176 (72). The interaction between the heavily glycosylated ACE2 and glycosylated S protein predicts a role for N-glycosylation in forming the receptor-S interaction. The published crystal structure and molecular modeling of hACE2 indicate that N90-, N322-, and N546-linked glycans interact with the SARS-CoV-2 S protein (19, 35, 36, 77). Other studies show that the absence of N-linked glycans in hACE2 has little or no effect on S binding (37, 38). Here, we show that the complete removal of N-glycans by mutagenesis or TM treatment did not disrupt the interaction of both ACE2 receptors (pig and human) with SARS-CoV or SARS-CoV-2 S proteins. Moreover, removal of all N-glycans on ACE2 and S proteins did not prevent coprecipitation, suggesting that glycans do not play a critical role in forming the interaction between ACE2 and S protein. In contrast, other studies have reported for other viruses an important role of the sialic acid present in the N-glycans on ligand-receptor interactions, including the coronavirus, such as the Middle East respiratory syndrome virus/MERS (78), parvovirus (79), and influenza (80, 81).

Interestingly, our immunofluorescence results showed localization of ACE2 and spike in the cytoplasm and in the plasma membrane (Fig. 6B and Fig. 7F), suggesting that hACE2 and S protein might also interact early after their biogenesis. The association of both proteins in cytoplasmic regions that resemble the ER is clearly evident in our colocalization studies in which the ACE2 and/or spike were deglycosylated (Fig. 7F and G). These observations align with our findings that showed that the removal of the N-glycosylation sites, by TM treatment or mutagenesis, induces ACE2 retention in the ER (Fig. 2 and 3). Similar results were observed for pACE2. However, in this case, pACE2 and S protein mostly colocalized in ER-resembling cytoplasmic structures, suggesting that pACE2 and S protein associate in early stages after their biosynthesis (Fig. 6 and Fig. 7F).

In agreement with previous studies, we found that the removal of N-glycans from hACE2 decreased the fusogenic ability of the viral S protein from SARS-CoV (Fig. 9A and C) (59). One likely explanation for reduced fusogenic activity is the decreased surface expression of deglycosylated ACE2. Under the same experimental conditions, SARS-CoV-2 S protein did not lose the ability to mediate cell-to-cell membrane fusion. This observation is consistent with previous reports that demonstrated that the higher ability to mediate cell-cell fusion of the SARS-CoV-2 S protein is likely due to the presence of a furin cleavage site in its sequence (27, 61, 65). In agreement with this notion, insertion of the S1/S2 furin cleavage site significantly potentiated the capacity of SARS-CoV S protein to mediate cell-cell fusion but did not affect virion entry (82). In general, the S1/S2 furin-recognition site is missing in most  $\beta$ -B coronaviruses, and their S proteins are uncleaved in normal conditions. For instance, in the case of SARS-CoV, which uses mainly the endosomal membrane fusion pathway to enter the host cell, its S protein is cleaved by endosomal cathepsin L and activated (83–85). The specific role of the S1/S2 cleavage site in the viral life cycle of SARS-CoV-2 needs further investigation. A recent study revealed that furin promotes both SARS-CoV-2 infectivity and cell-cell spread but it is not absolutely essential for SARS-CoV-2 infection, and replication occurs in its absence, suggesting that furin-targeting drugs may reduce but not abolish viral spread (27). In line with these observations, a possible role of the furin cleavage site in reducing SARS-CoV-2 sensitivity to innate immune restriction was also proposed (86). Even though the role of the furin cleavage site in the SARS-CoV-2 life

cycle remains unclear, in this study we demonstrated that it might function to overcome the low cell surface expression of deglycosylated ACE2. The high ACE2-binding affinity of the SARS-CoV-2 S protein is another important characteristic that could explain why this protein did not lose the capacity to mediate cell-to-cell membrane fusion in cells expressing the hACE2\* mutant (19, 57, 77, 87–89). The ACE2-binding affinity of the receptor-binding domain (RBD) of the S protein of SARS-CoV-2 is higher than that of SARS-CoV, which may contribute to the ability of the SARS-CoV-2 S protein to mediate membrane fusion in a manner that surpasses the capacity of SARS-CoV (19, 57, 77, 87–89).

Our findings indicated that hACE2 N-glycosylation is required to allow an efficient viral entry of both SARS-CoV and SARS-CoV-2 virus, which can be attributed to the fact that N-glycosylation is necessary for the proper cell surface expression of hACE2. In agreement with this notion, normalization of cell surface expression of hACE2 to a level similar to that of hACE2\* resulted in a decline in viral entry for both coronaviruses (Fig. 10B and C), which confirms that the drop in viral entry is probably due to the lack of available cell surface hACE2. Another possible explanation is that the removal of the N-glycans induced a misfolding of the hACE2 glycoprotein. However, our binding S-ACE2 experiments and protease activity studies suggested that N-glycosylation-deficient ACE2 variants are properly folded (Fig. 5, 7, and 8). Alteration of N-linked glycans in ACE2 blocked its ability to support the transduction of SARS-CoV and human coronavirus NL63 (HCoV-NL63) S pseudotyped viruses by disruption of the viral S protein-induced membrane fusion (59). It remains to be determined whether the reduced fusogenic activity is due to the aberrant glycan structure of ACE2 or to the misfolding of the glycoprotein.

By analyzing the effect of blocking complex N-glycans' formation of hACE2 receptor, it has been proposed that ACE2 glycans may not regulate viral entry of SARS-CoV-2 (38). In contrast to a full inhibition of N-glycosylation biosynthesis, our data showed that inhibition of complex N-glycosylation (by using KIF) did not alter the cell surface expression of ACE2. Moreover, a whole N-glycosylation depletion of the ACE2 receptor did not disrupt the S-ACE2 interaction, which would explain why the ACE2 N-glycans do not have a role in the viral entry of SARS-CoV-2. These observations support the idea that the reduction of viral entry in cells expressing a nonglycosylated ACE2 is probably due to the lack of available cell surface ACE2. However, the N-linked sugars present on the S protein were critical for the virus to enter the host cells, since inhibition of complex N-glycan biosynthesis enhanced S protein proteolysis, suggesting that N-glycosylation might play a role in regulating SARS-CoV-2 S protein stability (38, 39). In agreement with these findings, we observed that the expression of a nonglycosylated S variant was very low and was detected by Western blotting only when it was coprecipitated with ACE2, indicating that the blocking of N-glycosylation might affect the stability or expression of the S protein.

Our findings indicated that N-glycosylation is required for efficient protein expression of ACE2. However, the exact role of N-linked glycosylation in the protein expression remains to be determined. Similarly, it was shown that the expression levels of other receptors, such as rhodopsin (90),  $\beta$ 2-adrenergic receptor (91), angiotensin II type-1 receptor (75), and the orphan G protein-coupled receptor Gpr176 (72), were all reduced by the depletion of N-glycosylation. However, this does not necessarily hold true for other receptors; for instance, it was shown that the expression levels of the orphan GPCR Gpr6 (92),  $\alpha$ 1-adrenergic receptor (93), M2 muscarinic receptor (94), histamine H2 receptor (76), vasopressin V2 receptor (95), PTH receptor (96), LH-RH receptor (97), and oxytocin receptor (98) were not significantly modified by the blocking of N-glycosylation.

There is a body of work describing the antiviral effect of N-glycosylation inhibitors on coronavirus infection by affecting CoV S-glycoprotein function (99–101). Our results showed that treatment of cells with the N-glycosylation inhibitor tunicamycin drastically reduced the cell surface expression of ACE2. Therefore, it would be important to identify N-glycosylation inhibitors with safety profiles in humans or animals that

decrease cell membrane expression of ACE2 and evaluate their effect in regulating viral entry. Potential N-glycosylation inhibitors that can be tested might include swainsonine, which has a demonstrated safety profile in humans (102),  $\alpha$ -mannosidase inhibitors (48), and  $\alpha$ -glucosidase inhibitors (99, 101), such as castanospermine and celgosivir, which have been shown to inhibit SARS-CoV-2 replication (99). The results of these studies will determine whether inhibiting or reducing cell surface availability of ACE2 may provide a novel antiviral therapy to regulate viral entry and reduce coronavirus-related disease transmission. In addition, the results could identify dual-benefit drugs that inhibit both ACE2 and S protein functions during infection.

## MATERIALS AND METHODS

**Plasmids.** The plasmids pCDNA3.1-hACE2-FLAG and pCDNA3.1-pACE2-FLAG, which express human ACE2 (GenBank accession number [NM\\_021804.3](#)) and pig ACE2 (GenBank accession number [NM\\_001123070.1](#)) fused to a FLAG epitope, respectively, were purchased from GenScript, as well as the pCDNA3.1-TMPRSS2-FLAG expressing TMPRSS2 (GenBank accession number [NM\\_005656.4](#)) fused to a FLAG epitope. pCDNA3.1-SARS2-spike expressing full-length spike (S) protein from SARS-CoV-2 (GenBank accession number [QHD43416.1](#)) was purchased from Addgene. Expression plasmid encoding S protein from SARS-CoV (GenBank accession number [AAP13567.1](#)) was purchased from SinoBiological. pCDNA3.1-SARS2-spike  $\Delta$ 19 expressing a truncated SARS-CoV2 spike protein with the last 19 amino acids removed was generated by using the Q5 site-directed mutagenesis kit (New England Biolabs), the plasmid pCDNA3.1-SARS2-spike, and the following mutagenic oligonucleotide primers: the sense primer, 5'-CAGCTGCTGCTAGTTCTGATGAGGACG-3', and the antisense primer, 5'-CCGCAGGAGCAGAGCCC-3', following the manufacturer's recommendations.

The pCDNA3.1-hACE2-FLAG plasmid and a Q5 site-directed mutagenesis kit (New England Biolabs) were used according to the manufacturer's specifications to generate recombinant plasmids that expressed hACE2 N-glycosylation mutants, by substituting the N-linking site with Q. The following mutagenic oligonucleotide primers were used: for the production of mutation N53Q, the sense primer was 5'-TTATAACACCCAAATTAAGAGAGATG-3' and the antisense primer was 5'-TTCCAAGAAGCAAGTGAAC-3', for the production of mutation N103Q, the sense primer was 5'-TCTTCAGCAACAAGGGTCTTCAGTGC-3' and the antisense primer was 5'-GCCTGCAGCTGAAGCTTG-3', for the production of mutation N90Q, the sense primer was 5'-AGAAATTCAGCAGCTCACAGTCAAG-3' and the antisense primer was 5'-TGTAGTGGATACATTTGG-3', for the production of mutation N322Q, the sense primer was 5'-TGGTCTTCTCAGATGACTCAAG-3' and the antisense primer was 5'-ACAGATACAAGAAGTCTCTC-3', for the production of mutation N546Q, the sense primer was 5'-TGACATCTCACAGTCTACAGAAGCTG-3' and the antisense primer was 5'-CATTGTGCGAGGGCCT-3', for the production of mutation N432Q, the sense primer was 5'-TCAAGAAGACCAAGAAACAGAAATAAAGTTC-3' and the antisense primer was 5'-AAATCGGGTGACAGAAGAC-3', and for the production of mutation N690Q, the sense primer was 5'-TGCACCTAAACAAGTGTCTGATATC-3' and the antisense primer was 5'-GTGACAAAGAAATTAAGGAG-3'. The correctness of the constructs was confirmed by sequencing and by Western blotting of the expressed proteins. The hACE2\* is a mutant in which the Asn (N) for all consensus N-glycosylation sites was replaced with a Gln (Q).

**Cells, antibodies, and reagents.** HEK 293T cells (ATCC CRL-3216 from American Type Culture Collection, Rockville, MD) and HEK 293T Lenti-X (Clontech/TaKaRa Bio) were cultured at 37°C in 5% CO<sub>2</sub> in Dulbecco's modified Eagle's medium (DMEM; Life Technologies) supplemented with 10% fetal bovine serum (FBS; Gibco), 2 mM L-glutamine (Life Technologies), and antibiotics (100 U/ml penicillin and 100  $\mu$ g/ml streptomycin; Life Technologies).

The following reagents and their commercial sources were used: tunicamycin and cycloheximide (Sigma), Kifunensine (Tocris Bioscience), ACE2 activity kit (no. K897, BioVision), anti-FLAG-agarose beads (Sigma), and 3 $\times$  FLAG peptide (Sigma). The following antibodies were purchased from Thermo Fischer: SARS-CoV/SARS-CoV-2 spike protein S2 monoclonal antibody (1A9), protein disulfide-isomerase (PDI) mouse antibody (clone: RL90), and Alexa 594- and Alexa 488-conjugated antibodies against mouse and rabbit IgG, respectively. The monoclonal anti-FLAG M2 antibody was purchased from Sigma. The anti-GAPDH (anti-glyceraldehyde-3-phosphate dehydrogenase; D4C6R) monoclonal antibody, the golgin-97 (D8P2K) rabbit monoclonal antibody, the calnexin (C5C9) rabbit monoclonal antibody, and the FLAG tag (D6W5B) rabbit monoclonal antibody were from Cell Signaling. The human ACE2 Alexa Fluor 488-conjugated antibody (535919) was purchased from R&D systems.

**Transfection and immunofluorescence microscopy.** Transfections of cell monolayers were done with the TransIT-LT1 transfection reagent (Mirus) according to the manufacturer's instructions (Mirus). Transfected cells were incubated at 37°C for 24 to 48 h unless otherwise stated. For indirect immunofluorescence (IF) microscopy, cell monolayers grown on coverslips were transfected as indicated in the figure legends. At the indicated times, the monolayers were fixed with 4% paraformaldehyde. Fixed cells were permeabilized with 0.5% Triton X-100 in phosphate-buffered saline (PBS) and then blocked in PBS containing 2% bovine serum albumin. After incubation with primary antibodies for 1 h at RT or overnight at 4°C, the cells were incubated for 1 h with secondary antibodies and DAPI (4',6'-diamidino-2-phenylindole). Images were obtained with a Nikon A1R laser scanning confocal microscope. The images were processed with NIS-elements software (Nikon).

**Quantitative analysis of fluorescent images.** Five to six fields were randomly selected in each well to analyze 50 to 60 individual cells. The fluorescence intensity of individual cells was measured by NIS-element software. The channel for each specific fluorescent signal was analyzed and the regions of interest (individual cells) were selected. The colocalization analysis was performed by using the colocalization analysis tool of NIS-element software. In order to determine whether two fluorescent signals colocalized with each other, the Pearson's correlation coefficient (PCC) values of individual cells were measured (103). The PCC values between ACE2 proteins and ER marker staining were determined using NIS-elements software (104). Higher PCC values denoted higher levels of colocalization between the two fluorescent signals (see Fig. 2 and 3). Statistical analysis of the data was performed by using Student's *t* test. A *P* value of  $<0.05$  was considered to be statistically significant.

**Western blotting.** Cellular proteins were extracted with a whole-cell extract buffer (50 mM Tris [pH 7.5], 150 mM NaCl, 0.5% Triton X-100, 10% glycerol, 1 mM EDTA, protease inhibitor cocktail [Sigma]). Cells lysates were resolved on 4 to 12% Bis-Tris NuPAGE gels (Invitrogen) and transferred to nitrocellulose membranes using a trans-blot turbo transfer system (Bio-Rad). Protein bands were detected with specific antibodies using SuperSignal West femto maximum sensitivity substrate (Thermo Fisher) and viewed on a FluorChem R system (ProteinSimple).

**Immunoprecipitation assay.** Human 293T cells were independently transfected with plasmids encoding FLAG-tagged mutant and wild-type hACE2 proteins, FLAG-tagged pACE2 protein, and untagged SARS-CoV/SARS-CoV-2 S protein. For some experiments, cells were treated with tunicamycin (1  $\mu$ g/ml) for 16 h before harvesting. After 24 h, the cells expressing each ACE2 variant or S protein were lysed in 1 ml of whole-cell extract buffer. Lysates were centrifuged at 14,000 rpm for 30 min at 4°C. Post-spin lysates were then precleared using protein A-agarose (Sigma) for 1 h at 4°C; a small aliquot of each of these lysates was stored as an input sample. Precleared lysates containing the differently tagged or untagged proteins were mixed in a 1:1 ratio and incubated with anti-FLAG-agarose beads (Sigma) overnight at 4°C to precipitate the FLAG-tagged proteins. Beads containing the immunoprecipitate were washed four times in whole-cell extract buffer. Subsequently, immune complexes were eluted using 200  $\mu$ g of 3 $\times$  FLAG peptide/ml in whole-cell extract buffer without Triton X-100. The eluted samples were separated by SDS-PAGE and analyzed by Western blotting using anti-FLAG M2 monoclonal antibody or SARS-CoV/SARS-CoV-2 spike protein S2 monoclonal antibody.

**Cell surface biotinylation assay.** Human 293T cells were transiently transfected with plasmids encoding FLAG-tagged hACE2 variants or FLAG-tagged pACE2 protein for 24 h. Where indicated, cells were treated with tunicamycin (1  $\mu$ g/ml) for 16 h before harvesting. The cell surface biotinylation assay was performed using the Pierce cell surface biotinylation and isolation kit (Thermo Fisher) following the manufacturer's recommendations. Briefly, the cell surface of 293T cells was biotinylated using EZ-Link sulfo-NHS-SS-biotin. Cells were lysed with whole-cell extract buffer and biotinylated proteins were recovered with Neutravidin beads. Input lysates and pulldown proteins were analyzed by Western blotting with the anti-FLAG M2 monoclonal antibody (Sigma) and anti-GAPDH monoclonal antibody (Cell Signaling) as described above.

**ACE2 activity assay.** Human 293T cells were transiently transfected with 10  $\mu$ g of plasmid encoding FLAG-tagged hACE2 variants or FLAG-tagged pACE2 protein. Where indicated after transfection, cells were treated with tunicamycin (1  $\mu$ g/ml) for 16 h before harvesting. At 24 h posttransfection, cells were lysed with whole-cell extract buffer and the FLAG-tagged proteins were immunoprecipitated overnight at 4°C using anti-FLAG-agarose beads (Sigma), as described above. The immunoprecipitated extracts were processed in triplicates using the kit reagents and recommendations. The carboxypeptidase activity of the ACE2 variants was measured as fluorescence (excitation wavelength/emission wavelength [Ex/Em] = 320/420 nm) in kinetic mode using a Spectramax-ID5 plate reader (molecular devices) for 30 min to 2 h. A positive control was included by the kit. Immunoprecipitated extracts were also analyzed by Western blotting with the anti-FLAG M2 monoclonal antibody (Sigma) as described above.

**Flow cytometry analysis.** Flow cytometry was performed to quantify the GFP-positive cells after SARS-CoV-2 or SARS-CoV S pseudotyped virus infection. Monolayers of 293T cells expressing hACE2 variants were infected for 48 to 72 h at 37°C with either SARS-CoV-2 or SARS-CoV S pseudotyped virus. Infection was performed in the presence of 8  $\mu$ g/ml Polybrene. HEK 293T cells transfected with an empty plasmid were used as the background negative control. After 48 to 72 h postinfection, cells were gently trypsinized (trypsin-EDTA). The percentage of GFP-positive cells was determined by flow cytometry (Cytek Aurora). 293T cells were initially analyzed by light scattering, where forward scatter (FSC) is a measure of size and side scatter (SSC) is an indication of granularity and internal complexity. In all cases, a gate was applied on the bulk of the cells (95%), which excluded large aggregates. For each sample, 50,000 to 100,000 single cells were analyzed. To detect GFP, the samples were excited with a 488-nm laser coupled to an emission filter allowing the 515 nm wavelengths to go through. To quantify the cell surface expression of hACE2, HEK 293T cells were transiently transfected with plasmids expressing hACE2 or hACE2\* proteins using the TransIT-LT1 transfection reagent (Mirus) according to the manufacturer's instructions. The cells were collected at 24 h posttransfection. Cells were detached with 1 mM EDTA in PBS, washed twice with flow cytometry staining buffer (R&D Systems), and blocked with human BD Fc Block (BD Pharmingen) for 15 min at room temperature. Then, cells were immunostained with a human ACE2 Alexa Fluor 488-conjugated antibody (535919, R&D Systems) at 1  $\mu$ g/10<sup>6</sup> cells for 30 min at room temperature and washed three times with flow cytometry staining buffer prior to analysis by flow cytometry (Cytek Aurora). For each sample, 100,000 single cells were analyzed. To detect Alexa 488, the samples were excited with a 488-nm laser coupled to an emission filter allowing the 515 nm wavelengths to go through. The percentage of hACE2-positive cells was calculated by comparison with unstained and stained empty plasmid-transfected samples. Positive cells were gated as described

previously (40), and the same gating strategy was applied in all experiments. Briefly, the main HEK 293T cell population was gated with SSC-A versus FSC-A. The selected cells were gated with FSC-H versus FSC-A for single cells. From that, ACE2 positive cells were gated with FSC-H versus Alexa 488. All the data were processed with FlowJoV10 software. All experiments were done in triplicate and repeated at least three times. Statistical analysis of the data was performed by using Student's *t* test. A *P* value of <0.05 was considered to be statistically significant.

**SARS-CoV-2 S pseudovirions production and viral entry.** SARS-CoV-2 or SARS-CoV spike protein pseudovirions were generated by replacing the vesicular stomatitis virus (VSV-G) envelope protein of 3rd generation lentivirus with a mutant S protein possessing a deletion of 19 amino acid residues at the C terminus. To generate these viruses, Lenti-X 293 T cells (TaKaRa Bio) grown in a 10-cm dish were transiently transfected with the following plasmids: 5  $\mu$ g of pLenti-GFP (Cell Biolabs), 6  $\mu$ g of psPAX2 and 0.9  $\mu$ g of pCMV-VSV-G (Cell Biolabs), or 0.9  $\mu$ g of pCDNA3.1-SARS2-spike  $\Delta$ 19 or 0.9  $\mu$ g of pCDNA3.1-SARS-spike using the TransIT-LT1 transfection reagent (Mirus) according to the manufacturer's instructions. After overnight incubation, the medium was replaced with complete medium (DMEM plus 10% FBS). At 48 to 72 h after transfection, the supernatant was harvested, centrifuged at  $800 \times g$  for 5 min to remove cell debris, filtered through a 0.45- $\mu$ m pore size polyvinylidene difluoride (PVDF) syringe filter (Millipore), aliquoted, and stored at  $-80^{\circ}\text{C}$  until use.

In order to transduce cells with pseudovirions, virus was added to either mock-transfected 293T or ACE2-transfected 293T cell lines at 24 h posttransfection. Infection was performed in the presence of 8  $\mu$ g/ml Polybrene. After overnight incubation, cells were washed and returned to culture for 48 h and then subjected to flow cytometry analysis. GFP fluorescence was monitored daily. All flow cytometry and microscopy data presented in this study correspond to the 48 to 72 h after transduction.

**Cell-cell fusion assay.** HEK 293T cells expressing mutant or wild-type hACE2 variants were used as target cells. In some cases, the target cells were also transiently expressing type II membrane serine protease TMPRSS2. To prepare effector cells expressing S protein from either SARS-CoV or SARS-CoV-2, HEK 293T cells were cotransfected with plasmids encoding S-glycoprotein and enhanced green fluorescent protein (eGFP). For SARS-CoV S protein-mediated cell fusion, cells were lifted with trypsin (0.25%) at 24 h posttransfection and overlaid on a monolayer of target cells at a ratio of approximately 1:1. For SARS-CoV-2 S protein-mediated cell fusion, cells were detached with 1 mM EDTA and overlaid on target cells at a ratio similar to that above. After 24 h of incubation, five fields were randomly selected in each well to count the number of nuclei in fused and unfused cells. Images of syncytia were obtained with a Nikon A1R laser scanning confocal microscope. All experiments were performed in triplicate and repeated at least three times. Statistical analysis of the data was performed by using Student's *t* test. A *P* value of <0.05 was considered to be statistically significant.

**Treatment with N-glycosylation processing inhibitors and glycosidases.** Tunicamycin (TM) and kifunensine (KIF) at a concentration of 1  $\mu$ g/ml and 5  $\mu$ g/ml, respectively, were used to inhibit N-glycosylation in transfected HEK 293T cells. Prior to treatment, cell lysates were mixed with glycoprotein-denaturing buffer (New England Biolabs) and incubated at  $100^{\circ}\text{C}$  for 10 min. To remove high-mannose oligosaccharides, cell lysates were treated with endoglycosidase H (endo H) (New England BioLabs) for 1 h at  $37^{\circ}\text{C}$ . Peptide-N-glycosidase F (PNGase F) (New England BioLabs) was used to remove all N-linked oligosaccharides for 1 h at  $37^{\circ}\text{C}$ . Digested proteins were analyzed by Western blotting with anti-M2 FLAG monoclonal antibody (Sigma).

**Cell viability assay.** Cell viability was determined by measuring the reduction of the water-soluble tetrazolium dye MTS [3-(4,5-dimethylthiazol-2-yl)-5-(3-carboxymethoxyphenyl)-2-(4-sulfophenyl)-2H-tetrazolium] (Promega) to water-soluble colored formazan product. We treated  $3 \times 10^4$  cells/well in a 96-well plate with serial dilutions of the indicated drugs. HEK 293T cells were incubated with tunicamycin or kifunensine for 16 h, 24 h, and 48 h at  $37^{\circ}\text{C}$ . After the incubation periods, 20  $\mu$ l MTS solution was added to each well for an additional 2 h at  $37^{\circ}\text{C}$ . The optical density was measured at 490 nm using a microplate reader. Mock-treated cells represent 100% viability.

**Quantification and statistical analysis.** Densitometric analysis of the blots was performed with ImageJ software (version 2.1.0, National Institutes of Health, USA). All data are presented as mean  $\pm$  standard deviation. The mean and standard deviation values were calculated using GraphPad Prism 7.0c. Statistical analysis was performed using two-tailed unpaired Student's *t* test. A *P* value of <0.05 was considered to be statistically significant. Number of repeats are specified in the figure legends.

## REFERENCES

- World Health Organization. 2020. World Health Organization coronavirus disease 2019 (COVID-19) situation report. <https://www.who.int/emergencies/diseases/novel-coronavirus-2019/situation-reports>.
- Zhu N, Zhang D, Wang W, Li X, Yang B, Song J, Zhao X, Huang B, Shi W, Lu R, Niu P, Zhan F, Ma X, Wang D, Xu W, Wu G, Gao GF, Tan W, China Novel Coronavirus Investigating and Research Team. 2020. A novel coronavirus from patients with pneumonia in China, 2019. *N Engl J Med* 382: 727–733. <https://doi.org/10.1056/NEJMoa2001017>.
- Wu F, Zhao S, Yu B, Chen Y-M, Wang W, Song Z-G, Hu Y, Tao Z-W, Tian J-H, Pei Y-Y, Yuan M-L, Zhang Y-L, Dai F-H, Liu Y, Wang Q-M, Zheng J-J, Xu L, Holmes EC, Zhang Y-Z. 2020. A new coronavirus associated with human respiratory disease in China. *Nature* 579:265–269. <https://doi.org/10.1038/s41586-020-2008-3>.
- Zhou P, Yang X-L, Wang X-G, Hu B, Zhang L, Zhang W, Si H-R, Zhu Y, Li B, Huang C-L, Chen H-D, Chen J, Luo Y, Guo H, Jiang R-D, Liu M-Q, Chen Y, Shen X-R, Wang X, Zheng X-S, Zhao K, Chen Q-J, Deng F, Liu L-L, Yan B, Zhan F-X, Wang Y-Y, Xiao G-F, Shi Z-L. 2020. A pneumonia outbreak associated with a new coronavirus of probable bat origin. *Nature* 579: 270–273. <https://doi.org/10.1038/s41586-020-2012-7>.
- Chen G, Wu D, Guo W, Cao Y, Huang D, Wang H, Wang T, Zhang X, Chen H, Yu H, Zhang X, Zhang M, Wu S, Song J, Chen T, Han M, Li S, Luo X, Zhao J, Ning Q. 2020. Clinical and immunological features of severe and moderate coronavirus disease 2019. *J Clin Invest* 130:2620–2629. <https://doi.org/10.1172/JCI137244>.
- Huang C, Wang Y, Li X, Ren L, Zhao J, Hu Y, Zhang L, Fan G, Xu J, Gu X, Cheng Z, Yu T, Xia J, Wei Y, Wu W, Xie X, Yin W, Li H, Liu M, Xiao Y, Gao H,

- Guo L, Xie J, Wang G, Jiang R, Gao Z, Jin Q, Wang J, Cao B. 2020. Clinical features of patients infected with 2019 novel coronavirus in Wuhan. *China Lancet* 395:497–506. [https://doi.org/10.1016/S0140-6736\(20\)30183-5](https://doi.org/10.1016/S0140-6736(20)30183-5).
7. Wang D, Hu B, Hu C, Zhu F, Liu X, Zhang J, Wang B, Xiang H, Cheng Z, Xiong Y, Zhao Y, Li Y, Wang X, Peng Z. 2020. Clinical characteristics of 138 hospitalized patients with 2019 novel coronavirus-infected pneumonia in Wuhan, China. *JAMA* 323:1061–1069. <https://doi.org/10.1001/jama.2020.1585>.
  8. Kwok KO, Huang Y, Tsoi MTF, Tang A, Wong SYS, Wei WI, Hui DSC. 2021. Epidemiology, clinical spectrum, viral kinetics and impact of COVID-19 in the Asia-Pacific region. *Respirology* 26:322–333. <https://doi.org/10.1111/resp.14026>.
  9. World Health Organization. 2020. Clinical management of COVID-19: interim guidance, 27 May 2020. World Health Organization, Geneva, Switzerland.
  10. Lillcrap D. 2020. Disseminated intravascular coagulation in patients with 2019-nCoV pneumonia. *J Thromb Haemost* 18:786–787. <https://doi.org/10.1111/jth.14781>.
  11. Song P, Li W, Xie J, Hou Y, You C. 2020. Cytokine storm induced by SARS-CoV-2. *Clin Chim Acta* 509:280–287. <https://doi.org/10.1016/j.cca.2020.06.017>.
  12. Zhao Z, Wei Y, Tao C. 2021. An enlightening role for cytokine storm in coronavirus infection. *Clin Immunol* 222:108615. <https://doi.org/10.1016/j.clim.2020.108615>.
  13. Teijaro JR, Farber DL. 2021. COVID-19 vaccines: modes of immune activation and future challenges. *Nat Rev Immunol* 21:195–197. <https://doi.org/10.1038/s41577-021-00526-x>.
  14. Kyriakidis NC, López-Cortés A, González EV, Grimaldos AB, Prado EO. 2021. SARS-CoV-2 vaccines strategies: a comprehensive review of phase 3 candidates. *NPJ Vaccines* 6:28. <https://doi.org/10.1038/s41541-021-00292-w>.
  15. Indari O, Jakhmola S, Elangovan M, Jha HC. 2021. An update on antiviral therapy against SARS-CoV-2: how far have we come? *Front Pharmacol* 12:632677. <https://doi.org/10.3389/fphar.2021.632677>.
  16. Hoffmann M, Kleine-Weber H, Schroeder S, Krüger N, Herrler T, Erichsen S, Schiergens TS, Herrler G, Wu N-H, Nitsche A, Müller MA, Drosten C, Pöhlmann S. 2020. SARS-CoV-2 cell entry depends on ACE2 and TMPRSS2 and is blocked by a clinically proven protease inhibitor. *Cell* 181:271–280.e8. <https://doi.org/10.1016/j.cell.2020.02.052>.
  17. Letko M, Marzi A, Munster V. 2020. Functional assessment of cell entry and receptor usage for SARS-CoV-2 and other lineage B betacoronaviruses. *Nat Microbiol* 5:562–569. <https://doi.org/10.1038/s41564-020-0688-y>.
  18. Walls AC, Park Y-J, Tortorici MA, Wall A, McGuire AT, Veesler D. 2020. Structure, function, and antigenicity of the SARS-CoV-2 spike glycoprotein. *Cell* 181:281–292.e6. <https://doi.org/10.1016/j.cell.2020.02.058>.
  19. Lan J, Ge J, Yu J, Shan S, Zhou H, Fan S, Zhang Q, Shi X, Wang Q, Zhang L, Wang X. 2020. Structure of the SARS-CoV-2 spike receptor-binding domain bound to the ACE2 receptor. *Nature* 581:215–220. <https://doi.org/10.1038/s41586-020-2180-5>.
  20. Clausen TM, Sandoval DR, Spliid CB, Pihl J, Perrett HR, Painter CD, Narayanan A, Majowicz SA, Kwong EM, McVicar RN, Thacker BE, Glass CA, Yang Z, Torres JL, Golden GJ, Bartels PL, Porell RN, Garretson AF, Laubach L, Feldman J, Yin X, Pu Y, Hauser BM, Caradonna TM, Kellman BP, Martino C, Gordts PLSM, Chanda SK, Schmidt AG, Godula K, Leibel SL, Jose J, Corbett KD, Ward AB, Carlin AF, Esko JD. 2020. SARS-CoV-2 infection depends on cellular heparan sulfate and ACE2. *Cell* 183:1043–1057.e15. <https://doi.org/10.1016/j.cell.2020.09.033>.
  21. Stadler K, Masignani V, Eickmann M, Becker S, Abrignani S, Klenk H-D, Rappuoli R. 2003. SARS—beginning to understand a new virus. *Nat Rev Microbiol* 1:209–218. <https://doi.org/10.1038/nrmicro775>.
  22. Ou X, Liu Y, Lei X, Li P, Mi D, Ren L, Guo L, Guo R, Chen T, Hu J, Xiang Z, Mu Z, Chen X, Chen J, Hu K, Jin Q, Wang J, Qian Z. 2020. Characterization of spike glycoprotein of SARS-CoV-2 on virus entry and its immune cross-reactivity with SARS-CoV. *Nat Commun* 11:1620. <https://doi.org/10.1038/s41467-020-15562-9>.
  23. Watanabe Y, Allen JD, Wrapp D, McLellan JS, Crispin M. 2020. Site-specific glycan analysis of the SARS-CoV-2 spike. *Science* 369:330–333. <https://doi.org/10.1126/science.abb9983>.
  24. Casalino L, Gaieb Z, Goldsmith JA, Hjorth CK, Dommer AC, Harbison AM, Fogarty CA, Barros EP, Taylor BC, McLellan JS, Fadda E, Amaro RE. 2020. Beyond shielding: the roles of glycans in the SARS-CoV-2 spike protein. *ACS Cent Sci* 6:1722–1734. <https://doi.org/10.1021/acscentsci.0c01056>.
  25. Hoffmann M, Kleine-Weber H, Pöhlmann S. 2020. A multibasic cleavage site in the spike protein of SARS-CoV-2 is essential for infection of human lung cells. *Mol Cell* 78:779–784.e5. <https://doi.org/10.1016/j.molcel.2020.04.022>.
  26. Shang J, Wan Y, Luo C, Ye G, Geng Q, Auerbach A, Li F. 2020. Cell entry mechanisms of SARS-CoV-2. *Proc Natl Acad Sci U S A* 117:11727–11734. <https://doi.org/10.1073/pnas.2003138117>.
  27. Papa G, Mallery DL, Albecka A, Welch LG, Cattin-Ortolá J, Luptak J, Paul D, McMahon HT, Goodfellow IG, Carter A, Munro S, James LC. 2021. Furin cleavage of SARS-CoV-2 Spike promotes but is not essential for infection and cell-cell fusion. *PLoS Pathog* 17:e1009246. <https://doi.org/10.1371/journal.ppat.1009246>.
  28. Matsuyama S, Ujike M, Morikawa S, Tashiro M, Taguchi F. 2005. Protease-mediated enhancement of severe acute respiratory syndrome coronavirus infection. *Proc Natl Acad Sci U S A* 102:12543–12547. <https://doi.org/10.1073/pnas.0503203102>.
  29. Wang W, McKinnin SMK, Farhan M, Paul M, McDonald T, McLean B, Llorens-Cortes C, Hazra S, Murray AG, Vederas JC, Oudit GY. 2016. Angiotensin-converting enzyme 2 metabolizes and partially inactivates pyr-apelin-13 and apelin-17: physiological effects in the cardiovascular system. *Hypertension* 68:365–377. <https://doi.org/10.1161/HYPERTENSIONAHA.115.06892>.
  30. Jiang F, Yang J, Zhang Y, Dong M, Wang S, Zhang Q, Liu FF, Zhang K, Zhang C. 2014. Angiotensin-converting enzyme 2 and angiotensin 1–7: novel therapeutic targets. *Nat Rev Cardiol* 11:413–426. <https://doi.org/10.1038/nrcardio.2014.59>.
  31. Chamsi-Pasha MA, Shao Z, Tang WW. 2014. Angiotensin-converting enzyme 2 as a therapeutic target for heart failure. *Curr Heart Fail Rep* 11: 58–63. <https://doi.org/10.1007/s11897-013-0178-0>.
  32. Tipnis SR, Hooper NM, Hyde R, Karran E, Christie G, Turner AJ. 2000. A human homolog of angiotensin-converting enzyme: cloning and functional expression as a captopril-insensitive carboxypeptidase. *J Biol Chem* 275:33238–33243. <https://doi.org/10.1074/jbc.M002615200>.
  33. Li W, Moore MJ, Vasilieva N, Sui J, Wong SK, Berne MA, Somasundaran M, Sullivan JL, Luzuriaga K, Greenough TC, Choe H, Farzan M. 2003. Angiotensin-converting enzyme 2 is a functional receptor for the SARS coronavirus. *Nature* 426:450–454. <https://doi.org/10.1038/nature02145>.
  34. Shajahan A, Archer-Hartmann SA, Supekar NT, Gleinich AS, Heiss C, Azadi P. 2020. Comprehensive characterization of N- and O-glycosylation of SARS-CoV-2 human receptor angiotensin converting enzyme 2. *bioRxiv*. <https://doi.org/10.1101/2020.05.01.071688>.
  35. Zhao P, Praissman JL, Grant OC, Cai Y, Xiao T, Rosenbalm KE, Aoki K, Kellman BP, Bridger R, Barouch DH, Brindley MA, Lewis NE, Tiemeyer M, Chen B, Woods RJ, Wells L. 2020. Virus-receptor interactions of glycosylated SARS-CoV-2 spike and human ACE2 receptor. *Cell Host Microbe* 28: 586–601.e6. <https://doi.org/10.1016/j.chom.2020.08.004>.
  36. Mehdipour AR, Hummer G. 2020. Dual nature of human ACE2 glycosylation in binding to SARS-CoV-2 spike. *bioRxiv*. <https://doi.org/10.1101/2020.07.09.193680>.
  37. Allen JD, Watanabe Y, Chawla H, Newby ML, Crispin M. 2021. Subtle influence of ACE2 glycan processing on SARS-CoV-2 recognition. *J Mol Biol* 433:166762. <https://doi.org/10.1016/j.jmb.2020.166762>.
  38. Yang Q, Hughes TA, Kelkar A, Yu X, Cheng K, Park S, Huang W-C, Lovell JF, Neelamegham S. 2020. Inhibition of SARS-CoV-2 viral entry upon blocking N- and O-glycan elaboration. *Elife* 9:e61552. <https://doi.org/10.7554/eLife.61552>.
  39. Azad T, Singaravelu R, Taha Z, Jamieson TR, Boulton S, Crupi MJF, Martin NT, Brown EEF, Poutou J, Ghahremani M, Pelin A, Nouri K, Rezaei R, Marshall CB, Enomoto M, Arulanandam R, Alluqmani N, Samson R, Gingras A-C, Cameron DW, Greer PA, Ilkow CS, Diallo J-S, Bell JC. 2021. Nanoluciferase complementation-based bioreporter reveals the importance of N-linked glycosylation of SARS-CoV-2 S for viral entry. *Mol Ther* 29:1984–2000. <https://doi.org/10.1016/j.ymthe.2021.02.007>.
  40. Conceicao C, Thakur N, Human S, Kelly JT, Logan L, Bialy D, Bhat S, Stevenson-Leggett P, Zagrajek AK, Hollinghurst P, Varga M, Tsigioti C, Tully M, Chiu C, Moffat K, Silesian AP, Hammond JA, Maier HJ, Bickerton E, Shelton H, Dietrich I, Graham SC, Bailey D. 2020. The SARS-CoV-2 Spike protein has a broad tropism for mammalian ACE2 proteins. *PLoS Biol* 18: e3001016. <https://doi.org/10.1371/journal.pbio.3001016>.
  41. Chen W, Yan M, Yang L, Ding B, He B, Wang Y, Liu X, Liu C, Zhu H, You B, Huang S, Zhang J, Mu F, Xiang Z, Feng X, Wen J, Fang J, Yu J, Yang H, Wang J. 2005. SARS-associated coronavirus transmitted from human to pig. *Emerg Infect Dis* 11:446–448. <https://doi.org/10.3201/eid1103.040824>.
  42. Pickering BS, Smith G, Pinette MM, Embury-Hyatt C, Moffat E, Marszal P, Lewis CE. 2021. Susceptibility of domestic swine to experimental infection with severe acute respiratory syndrome coronavirus 2. *Emerg Infect Dis* 27:104–112. <https://doi.org/10.3201/eid2701.203399>.

43. Weingartl HM, Copps J, Drebot MA, Marszal P, Smith G, Gren J, Andova M, Pasick J, Kitching P, Czub M. 2004. Susceptibility of pigs and chickens to SARS coronavirus. *Emerg Infect Dis* 10:179–184. <https://doi.org/10.3201/eid1002.030677>.
44. Shi J, Wen Z, Zhong G, Yang H, Wang C, Huang B, Liu R, He X, Shuai L, Sun Z, Zhao Y, Liu P, Liang L, Cui P, Wang J, Zhang X, Guan Y, Tan W, Wu G, Chen H, Bu Z. 2020. Susceptibility of ferrets, cats, dogs, and other domesticated animals to SARS–coronavirus 2. *Science* 368:1016–1020. <https://doi.org/10.1126/science.abb7015>.
45. Schlottau K, Rissmann M, Graaf A, Schön J, Sehl J, Wylezich C, Höper D, Mettenleiter TC, Balkema-Buschmann A, Harder T, Grund C, Hoffmann D, Breithaupt A, Beer M. 2020. SARS-CoV-2 in fruit bats, ferrets, pigs, and chickens: an experimental transmission study. *Lancet Microbe* 1: e218–e225. [https://doi.org/10.1016/S2666-5247\(20\)30089-6](https://doi.org/10.1016/S2666-5247(20)30089-6).
46. Bieberich E. 2014. Synthesis, processing, and function of N-glycans in N-glycoproteins, p 47–70. *In* Yu R, Schengrund CL (ed), *Glycobiology of the nervous system*. Advances in Neurobiology, vol 9. Springer, New York, NY.
47. Aebi M. 2013. N-linked protein glycosylation in the ER. *Biochim Biophys Acta* 1833:2430–2437. <https://doi.org/10.1016/j.bbamcr.2013.04.001>.
48. Esko JD, Bertozzi C, Schnaar RL. 2017. Chemical tools for inhibiting glycosylation. *In* Varki A, Cummings RD, Esko JD, Stanley P, Hart GW, Aebi M, Darvill AG, Kinoshita T, Packer NH, Prestegard JH, Schnaar RL, Seeberger PH. *Essentials of Glycobiology* [Internet], 3rd ed. Cold Spring Harbor, New York, NY.
49. Elbein AD, Tropea JE, Mitchell M, Kaushal GP. 1990. Kifunensine, a potent inhibitor of the glycoprotein processing mannosidase I. *J Biol Chem* 265: 15599–15605. [https://doi.org/10.1016/S0021-9258\(18\)55439-9](https://doi.org/10.1016/S0021-9258(18)55439-9).
50. Cory AH, Owen TC, Barltrop JA, Cory JG. 1991. Use of an aqueous soluble tetrazolium/formazan assay for cell growth assays in culture. *Cancer Commun* 3:207–212. <https://doi.org/10.3727/095535491820873191>.
51. Riss T. 1992. Comparison of MTT, XTT and a novel tetrazolium compound MTS for in-vitro proliferation and chemosensitivity assays. *Mol Biol Cell* 3:184–190.
52. Alenquer M, Vale-Costa S, Etibor TA, Ferreira F, Sousa AL, Amorim MJ. 2019. Influenza A virus ribonucleoproteins form liquid organelles at endoplasmic reticulum exit sites. *Nat Commun* 10:1629. <https://doi.org/10.1038/s41467-019-09549-4>.
53. Yen J-B, Wei L-H, Chen L-W, Chen L-Y, Hung C-H, Wang S-S, Chang P-J. 2018. Subcellular localization and functional characterization of GII. 4 norovirus-encoded NTPase. *J Virol* 92. <https://doi.org/10.1128/JVI.01824-17>.
54. Lei X, Dong X, Ma R, Wang W, Xiao X, Tian Z, Wang C, Wang Y, Li L, Ren L, Guo F, Zhao Z, Zhou Z, Xiang Z, Wang J. 2020. Activation and evasion of type I interferon responses by SARS-CoV-2. *Nat Commun* 11:3810–3812. <https://doi.org/10.1038/s41467-020-17665-9>.
55. Yan R, Zhang Y, Li Y, Xia L, Guo Y, Zhou Q. 2020. Structural basis for the recognition of SARS-CoV-2 by full-length human ACE2. *Science* 367: 1444–1448. <https://doi.org/10.1126/science.abb2762>.
56. Wan Y, Shang J, Graham R, Baric RS, Li F. 2020. Receptor recognition by the novel coronavirus from Wuhan: an analysis based on decade-long structural studies of SARS coronavirus. *J Virol* 94. <https://doi.org/10.1128/JVI.00127-20>.
57. Wrapp D, Wang N, Corbett KS, Goldsmith JA, Hsieh C-L, Abiona O, Graham BS, McLellan JS. 2020. Cryo-EM structure of the 2019-nCoV spike in the prefusion conformation. *Science* 367:1260–1263. <https://doi.org/10.1126/science.abb2507>.
58. Chan KK, Dorosky D, Sharma P, Abbasi SA, Dye JM, Kranz DM, Herbert AS, Procko E. 2020. Engineering human ACE2 to optimize binding to the spike protein of SARS coronavirus 2. *Science* 369:1261–1265. <https://doi.org/10.1126/science.abc0870>.
59. Zhao X, Guo F, Comunale MA, Mehta A, Sehgal M, Jain P, Cuconati A, Lin H, Block TM, Chang J, Guo J-T. 2015. Inhibition of endoplasmic reticulum-resident glucosidases impairs severe acute respiratory syndrome coronavirus and human coronavirus NL63 spike protein-mediated entry by altering the glycan processing of angiotensin I-converting enzyme 2. *Antimicrob Agents Chemother* 59:206–216. <https://doi.org/10.1128/AAC.03999-14>.
60. Coutard B, Valle C, de Lamballerie X, Canard B, Seidah N, Decroly E. 2020. The spike glycoprotein of the new coronavirus 2019-nCoV contains a furin-like cleavage site absent in CoV of the same clade. *Antiviral Res* 176:104742. <https://doi.org/10.1016/j.antiviral.2020.104742>.
61. Xia S, Lan Q, Su S, Wang X, Xu W, Liu Z, Zhu Y, Wang Q, Lu L, Jiang S. 2020. The role of furin cleavage site in SARS-CoV-2 spike protein-mediated membrane fusion in the presence or absence of trypsin. *Signal Transduct Target Ther* 5:92–93. <https://doi.org/10.1038/s41392-020-0184-0>.
62. Bestle D, Heindl MR, Limburg H, Van Lam van T, Pilgram O, Moulton H, Stein DA, Harges K, Eickmann M, Dolnik O, Rohde C, Klenk H-D, Garten W, Steinmetzer T, Böttcher-Friebertshäuser E. 2020. TMPRSS2 and furin are both essential for proteolytic activation of SARS-CoV-2 in human airway cells. *Life Science Alliance* 3. <https://doi.org/10.26508/lsa.202000786>.
63. Nguyen HT, Zhang S, Wang Q, Anang S, Wang J, Ding H, Kappes JC, Sodroski J. 2021. Spike glycoprotein and host cell determinants of SARS-CoV-2 entry and cytopathic effects. *J Virol* 95. <https://doi.org/10.1128/JVI.02304-20>.
64. Hörnich BF, Großkopf AK, Schlagowski S, Tenbusch M, Kleine-Weber H, Neipel F, Stahl-Hennig C, Hahn AS. 2021. SARS-CoV-2 and SARS-CoV spike-mediated cell-cell fusion differ in their requirements for receptor expression and proteolytic activation. *J Virol* 95. <https://doi.org/10.1128/JVI.00002-21>.
65. Xia S, Liu M, Wang C, Xu W, Lan Q, Feng S, Qi F, Bao L, Du L, Liu S, Qin C, Sun F, Shi Z, Zhu Y, Jiang S, Lu L. 2020. Inhibition of SARS-CoV-2 (previously 2019-nCoV) infection by a highly potent pan-coronavirus fusion inhibitor targeting its spike protein that harbors a high capacity to mediate membrane fusion. *Cell Res* 30:343–355. <https://doi.org/10.1038/s41422-020-0305-x>.
66. Lee HS, Qi Y, Im W. 2015. Effects of N-glycosylation on protein conformation and dynamics: Protein Data Bank analysis and molecular dynamics simulation study. *Sci Rep* 5:8926–8927. <https://doi.org/10.1038/srep08926>.
67. Jayaprakash NG, Suroliya A. 2017. Role of glycosylation in nucleating protein folding and stability. *Biochem J* 474:2333–2347. <https://doi.org/10.1042/BCJ20170111>.
68. Tannous A, Pisoni GB, Hebert DN, Molinari M. 2015. N-linked sugar-regulated protein folding and quality control in the ER. *Semin Cell Dev Biol* 41:79–89. <https://doi.org/10.1016/j.semcdb.2014.12.001>.
69. Weng T-Y, Chiu W-T, Liu H-S, Cheng H-C, Shen M-R, Mount DB, Chou C-Y. 2013. Glycosylation regulates the function and membrane localization of KCC4. *Biochim Biophys Acta* 1833:1133–1146. <https://doi.org/10.1016/j.bbamcr.2013.01.018>.
70. Singh R, Almutairi MM, Pacheco-Andrade R, Almiahuob MYM, Di Fulvio M. 2015. Impact of hybrid and complex N-Glycans on cell surface targeting of the endogenous chloride cotransporter Slc12a2. *Int J Cell Biol* 2015:505294. <https://doi.org/10.1155/2015/505294>.
71. Hayashi H, Yamashita Y. 2012. Role of N-glycosylation in cell surface expression and protection against proteolysis of the intestinal anion exchanger SLC26A3. *Am J Physiol Cell Physiol* 302:C781–C795. <https://doi.org/10.1152/ajpcell.00165.2011>.
72. Wang T, Nakagawa S, Miyake T, Setsu G, Kunisue S, Goto K, Hirasawa A, Okamura H, Yamaguchi Y, Doi M. 2020. Identification and functional characterisation of N-linked glycosylation of the orphan G protein-coupled receptor Gpr176. *Sci Rep* 10:4429. <https://doi.org/10.1038/s41598-020-61370-y>.
73. Lee K-H, Ahn J-I, Yu D-H, Jeong H-S, Lee S-H, Kim K-S, Chung I-Y, Kim J-H, Lee Y-S. 2001. Effect of N-glycosylation on ligand binding affinity of rat V1a vasopressin receptor. *Biochem Biophys Res Commun* 286:707–713. <https://doi.org/10.1006/bbrc.2001.5456>.
74. Zhong X, Kriz R, Seehra J, Kumar R. 2004. N-linked glycosylation of platelet P2Y12 ADP receptor is essential for signal transduction but not for ligand binding or cell surface expression. *FEBS Lett* 562:111–117. [https://doi.org/10.1016/S0014-5793\(04\)00191-7](https://doi.org/10.1016/S0014-5793(04)00191-7).
75. Deslauriers B, Ponce C, Lombard C, Larguier R, Bonnafous J-C, Marie J. 1999. N-glycosylation requirements for the AT1a angiotensin II receptor delivery to the plasma membrane. *Biochem J* 339:397–405. <https://doi.org/10.1042/0264-6021:3390397>.
76. Fukushima Y, Oka Y, Saitoh T, Katagiri H, Asano T, Matsuhashi N, Takata K, Van Breda E, Yazaki Y, Sugano K. 1995. Structural and functional analysis of the canine histamine H2 receptor by site-directed mutagenesis: N-glycosylation is not vital for its action. *Biochem J* 310 (Pt 2):553–558. <https://doi.org/10.1042/bj3100553>.
77. Shang J, Ye G, Shi K, Wan Y, Luo C, Aihara H, Geng Q, Auerbach A, Li F. 2020. Structural basis of receptor recognition by SARS-CoV-2. *Nature* 581:221–224. <https://doi.org/10.1038/s41586-020-2179-y>.
78. Li W, Hulswit RJG, Widjaja I, Raj VS, McBride R, Peng W, Widagdo W, Tortorici MA, van Dieren B, Lang Y, van Lent JWM, Paulson JC, de Haan CAM, de Groot RJ, van Kuppeveld FJM, Haagmans BL, Bosch B-J. 2017. Identification of sialic acid-binding function for the Middle East respiratory syndrome coronavirus spike glycoprotein. *Proc Natl Acad Sci U S A* 114:E8508–E8517. <https://doi.org/10.1073/pnas.1712592114>.

79. Löfling J, Lyi SM, Parrish CR, Varki A. 2013. Canine and feline parvoviruses preferentially recognize the non-human cell surface sialic acid N-glycolylneuraminic acid. *Virology* 440:89–96. <https://doi.org/10.1016/j.virol.2013.02.009>.
80. Stencel-Baerenwald JE, Reiss K, Reiter DM, Stehle T, Dermody TS. 2014. The sweet spot: defining virus–sialic acid interactions. *Nat Rev Microbiol* 12:739–749. <https://doi.org/10.1038/nrmicro3346>.
81. Watanabe Y, Bowden TA, Wilson IA, Crispin M. 2019. Exploitation of glycosylation in enveloped virus pathobiology. *Biochim Biophys Acta Gen Subj* 1863:1480–1497. <https://doi.org/10.1016/j.bbagen.2019.05.012>.
82. Follis KE, York J, Nunberg JH. 2006. Furin cleavage of the SARS coronavirus spike glycoprotein enhances cell–cell fusion but does not affect virion entry. *Virology* 350:358–369. <https://doi.org/10.1016/j.virol.2006.02.003>.
83. Belouzard S, Chu VC, Whittaker GR. 2009. Activation of the SARS coronavirus spike protein via sequential proteolytic cleavage at two distinct sites. *Proc Natl Acad Sci U S A* 106:5871–5876. <https://doi.org/10.1073/pnas.0809524106>.
84. Huang I-C, Bosch BJ, Li F, Li W, Lee KH, Ghiran S, Vasilieva N, Dermody TS, Harrison SC, Dormitzer PR, Farzan M, Rottier PJM, Choe H. 2006. SARS coronavirus, but not human coronavirus NL63, utilizes cathepsin L to infect ACE2-expressing cells. *J Biol Chem* 281:3198–3203. <https://doi.org/10.1074/jbc.M508381200>.
85. Simmons G, Gosalia DN, Rennekamp AJ, Reeves JD, Diamond SL, Bates P. 2005. Inhibitors of cathepsin L prevent severe acute respiratory syndrome coronavirus entry. *Proc Natl Acad Sci U S A* 102:11876–11881. <https://doi.org/10.1073/pnas.0505577102>.
86. Winstone H, Lista MJ, Reid AC, Bouton C, Pickering S, Galao RP, Kerridge C, Doores KJ, Swanson CM, Neil SJ. 2021. The polybasic cleavage site in SARS-CoV-2 spike modulates viral sensitivity to type I interferon and IFITM2. *J Virol* 95. <https://doi.org/10.1128/JVI.02422-20>.
87. Wang Q, Zhang Y, Wu L, Niu S, Song C, Zhang Z, Lu G, Qiao C, Hu Y, Yuen K-Y, Wang Q, Zhou H, Yan J, Qi J. 2020. Structural and functional basis of SARS-CoV-2 entry by using human ACE2. *Cell* 181:894–904.e9. <https://doi.org/10.1016/j.cell.2020.03.045>.
88. Lu J, Sun PD. 2020. High affinity binding of SARS-CoV-2 spike protein enhances ACE2 carboxypeptidase activity. *J Biol Chem* 295:18579–18588. <https://doi.org/10.1074/jbc.RA120.015303>.
89. Jafari F, Jafari S, Ganjalikhany MR. 2021. In silico investigation of critical binding pattern in SARS-CoV-2 spike protein with angiotensin-converting enzyme 2. *Sci Rep* 11:6927. <https://doi.org/10.1038/s41598-021-86380-2>.
90. Kaushal S, Ridge KD, Khorana HG. 1994. Structure and function in rhodopsin: the role of asparagine-linked glycosylation. *Proc Natl Acad Sci U S A* 91:4024–4028. <https://doi.org/10.1073/pnas.91.9.4024>.
91. Rands E, Candelore M, Cheung A, Hill WS, Strader C, Dixon R. 1990. Mutational analysis of beta-adrenergic receptor glycosylation. *J Biol Chem* 265:10759–10764. [https://doi.org/10.1016/S0021-9258\(18\)87012-0](https://doi.org/10.1016/S0021-9258(18)87012-0).
92. Koziolewicz P, Alomar H, Yusof S, Grafton G, Cooper AJ, Curnow SJ, Ironside JW, Pall H, Barnes NM. 2017. N-glycosylation and expression in human tissues of the orphan GPR61 receptor. *FEBS Open Bio* 7: 1982–1993. <https://doi.org/10.1002/2211-5463.12339>.
93. Sawutz DG, Lanier SM, Warren CD, Graham RM. 1987. Glycosylation of the mammalian alpha 1-adrenergic receptor by complex type N-linked oligosaccharides. *Mol Pharmacol* 32:565–571.
94. van Koppen CJ, Nathanson NM. 1990. Site-directed mutagenesis of the m2 muscarinic acetylcholine receptor. Analysis of the role of N-glycosylation in receptor expression and function. *J Biol Chem* 265:20887–20892. [https://doi.org/10.1016/S0021-9258\(17\)45299-9](https://doi.org/10.1016/S0021-9258(17)45299-9).
95. Innamorati G, Sadeghi H, Birnbaumer M. 1996. A fully active nonglycosylated V2 vasopressin receptor. *Mol Pharmacol* 50:467–473.
96. Bisello A, Greenberg Z, Behar V, Rosenblatt M, Suva LJ, Chorev M. 1996. Role of glycosylation in expression and function of the human parathyroid hormone/parathyroid hormone-related protein receptor. *Biochemistry* 35:15890–15895. <https://doi.org/10.1021/bi962111j>.
97. Davis DP, Rozell TG, Liu X, Segaloff DL. 1997. The six N-linked carbohydrates of the lutropin/choriogonadotropin receptor are not absolutely required for correct folding, cell surface expression, hormone binding, or signal transduction. *Mol Endocrinol* 11:550–562. <https://doi.org/10.1210/mend.11.5.9927>.
98. Kimura T, Makino Y, Bathgate R, Iwell R, Nobunaga T, Kubota Y, Kumazawa I, Saji F, Murata Y, Nishihara T, Hashimoto M, Kinoshita M. 1997. The role of N-terminal glycosylation in the human oxytocin receptor. *Mol Hum Reprod* 3: 957–963. <https://doi.org/10.1093/molehr/3.11.957>.
99. Clarke EC, Nofchissey RA, Ye C, Bradfute SB. 2021. The iminosugars celgosivir, castanospermine and UV-4 inhibit SARS-CoV-2 replication. *Glycobiology* 31:378–384. <https://doi.org/10.1093/glycob/cwaa091>.
100. Santopolo S, Riccio A, Santoro MG. 2021. The biogenesis of SARS-CoV-2 spike glycoprotein: multiple targets for host-directed antiviral therapy. *Biochem Biophys Res Commun* 538:80–87. <https://doi.org/10.1016/j.bbrc.2020.10.080>.
101. Williams SJ, Goddard-Borger ED. 2020.  $\alpha$ -glucosidase inhibitors as host-directed antiviral agents with potential for the treatment of COVID-19. *Biochem Soc Trans* 48:1287–1295. <https://doi.org/10.1042/BST20200505>.
102. Goss PE, Reid CL, Bailey D, Dennis JW. 1997. Phase IB clinical trial of the oligosaccharide processing inhibitor swainsonine in patients with advanced malignancies. *Clinical Cancer Res* 3:1077–1086.
103. Dunn KW, Kamocka MM, McDonald JH. 2011. A practical guide to evaluating colocalization in biological microscopy. *Am J Physiol Cell Physiol* 300:C723–C742. <https://doi.org/10.1152/ajpcell.00462.2010>.
104. Huang L, Zhang Y, Xu C, Gu X, Niu L, Wang J, Sun X, Bai X, Xuan X, Li Q, Shi C, Yu B, Miller H, Yang G, Westerberg LS, Liu W, Song W, Zhao X, Liu C. 2017. Rictor positively regulates B cell receptor signaling by modulating actin reorganization via ezrin. *PLoS Biol* 15:e2001750. <https://doi.org/10.1371/journal.pbio.2001750>.